Check for updates

RESEARCH ARTICLE SUMMARY

IMMUNE SIGNALING

Disordered protein LAT encodes relative levels of signaling pathways in T cell activation

Adam J. Rubin*, Tyler T. Dao, Amelia V. Schueppert, Saehyun Choi, Jay T. Groves, Aviv Regev*, Alex K. Shalek*

Full article and list of author affiliations: https://doi.org/10.1126/science.ads6847

INTRODUCTION: Mapping the relationship between protein sequence and function is a fundamental problem in biology. This is especially challenging for proteins that engage in multiple molecular activities, raising the question of how distinct functions can be interwoven in a single sequence. Through multiple binding and biophysical functional sequence features, disordered proteins are known to organize large higher-order assemblies in ways that remain poorly understood.

RATIONALE: Experimental mapping of protein sequence-function relationships through large numbers of genetic perturbations has been limited to individual functional measures that fail to capture the complex behaviors of many proteins. We addressed this gap by developing perturbation-indexed, single-cell genetic screens that couple the exploratory power of traditional genetic approaches with information-rich, high-dimensional genomic readouts. As a representative case, we explored the problem of how linker for activation of T cells (LAT), a disordered adapter protein, achieves signal branching in T cell activation. Immune cells generally must sense environmental signals and convert that information into complex, well-regulated intracellular responses through numerous downstream pathways. To capture this process for LAT, we coupled mutation scanning to multiple genomic readouts that together monitor the process of T cell activation across regulatory layers.

RESULTS: Measuring epigenetic, transcriptomic, and cell surface protein dynamics of single cells harboring distinct LAT mutants, we found functional regions spanning more than 40% of the LAT amino acid sequence. Conserved sequence motifs for protein interactions, along with numerous sites of posttranslational modification, were critical sequence features and contributed to the interpretation of human genetic variation in LAT. Mutating critical sites of tyrosine phosphorylation and membrane-proximal regions required for cell surface trafficking conferred a near-complete loss of activation, whereas mutating a broader collection of sites had more moderate defects. Beyond short, conserved segments, patterned clusters of negatively charged residues were conserved independent of primary sequence and exhibited broad effects on T cell activation.

LAT mutants disrupting the AP-1 signaling pathway generally affected the nuclear factor of activated T cells (NFAT) pathway to a similar extent. To understand the molecular basis for this observation, we employed computational protein interaction modeling, protein proximity labeling, and imaging to monitor the composition of the LAT signalosome and the consequences of mutating critical sequence features. These results demonstrated that disruption of LAT interaction with a single partner protein indirectly disrupted other partner interactions, likely through the dual roles of these proteins as effectors of downstream pathways and bridging factors between LAT molecules.

CONCLUSION: Given the similarity of LAT to other disordered protein adapter-effector signaling systems, this signal balancing mechanism may be a general paradigm to constrain signaling outputs. Future efforts will be required to understand how distinct adaptive and innate immune responses are organized to achieve optimal pathway balance, noise tolerance, and kinetics, among other features encoded in adapter-effector systems. More broadly, we describe an extendable approach for interrogating sequence-function relationships for proteins with complex activities across regulatory layers of the cell. □

*Corresponding author. Email: adam@broadinstitute.org (A.J.R.); aviv.regev.sc@gmail.com (A.R.); shalek@mit.edu (A.K.S.) Cite this article as: A.J. Rubin *et al.*, *Science* **392**, eaea8782 (2026). DOI:10.1126/science.aea8782

Downloaded from https://www.science.org at Broad Institute on April 30, 2026

High-content genetic screen interrogates signal branching through a disordered protein assembly. We explored the problem of how the disordered protein linker for activation of T cells (LAT) achieves signal branching using single-cell genomic analyses of a pool of cells bearing mutations in the LAT gene. LAT contains numerous functional sequence elements that each influence multiple downstream signaling pathways in a coordinated manner. A model of LAT clustering organized by multiple effector proteins with dual roles as bridging molecules explains these observations. [Figure created using Adobe Illustrator and BioRender.com]

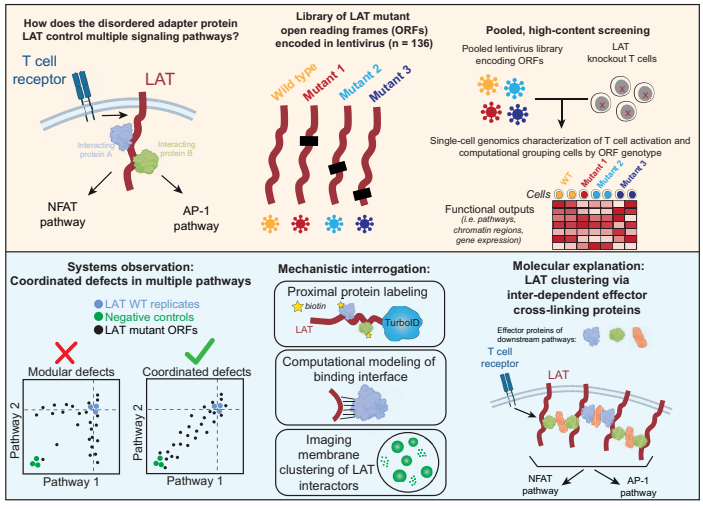

IMMUNE SIGNALING

Disordered protein LAT encodes relative levels of signaling pathways in T cell activation

Adam J. Rubin[1,2,3]*†, Tyler T. Dao[1,2,3,4]†, Amelia V. Schueppert[1,2,3], Saehyun Choi[5], Jay T. Groves[5], Aviv Regev[1,6]*‡¶, Alex K. Shalek[1,2,3]*‡

The disordered adapter protein linker for activation of T cells (LAT) propagates T cell receptor signaling. To interrogate how LAT coordinates multiple downstream pathways, we developed a single-cell screening approach, identifying widespread functional segments including protein interaction motifs and blocks of negative charge. Regardless of their position in LAT, individual segments generally conferred defects across all downstream signaling pathways. To understand the underlying mechanism, we used molecular biology, computational modeling, and imaging to demonstrate that disruption of LAT interaction with a single partner protein indirectly disrupts other partner interactions, likely through the dual roles of these proteins as effectors of downstream signaling and bridging factors between LAT molecules. Overall, we describe an extendable approach for interrogating sequence-function relationships for proteins with complex activities.

The T cell receptor (TCR) detects peptides bound to human leukocyte antigen (HLA) on antigen-presenting cells. This event initiates the complex response of T cell activation involving signaling pathway activity, chromatin remodeling, transcription, and the expression of effector proteins (*1*, *2*). The engaged TCR recruits the kinases lymphocyte-specific protein tyrosine kinase (LCK) and zeta-chain-associated protein kinase 70 (ZAP70), leading to phosphorylation and activation of the transmembrane protein linker for activation of T cells (LAT) (*2*, *3*). By organizing a collection of protein interactors, the extended disordered cytoplasmic tail of LAT relays the single channel signal of peptide-HLA sensing to activation of diverse downstream pathways, including nuclear factor of activated T cells (NFAT) and activator protein 1 (AP-1) (Fig. 1A) (*4*, *5*). Comparisons of LAT to other signaling proteins have identified critical sites of tyrosine phosphorylation and residues required for localization to the plasma membrane; other functional regions, meanwhile, have been nominated through consideration of known protein interaction determinants and potential sites of post-translational modification (*6*–*9*). The extent to which other regions of the LAT protein encode function and how all functional regions contribute to downstream pathway activity are not known.

Disordered protein regions, such as the LAT cytoplasmic domain, are present in roughly half of the proteome and commonly mediate signal branching (*10*, *11*). These regions can populate an ensemble of conformations, influenced by promiscuous interactions with structured proteins through numerous short linear motifs (SLiMs) (*12*). Recent efforts leveraging evolutionary sequence data and large-scale functional annotation (*13*, *14*), as well as comprehensive experimental interrogation of a single function to generate training data (*15*, *16*), have enabled the prediction of function for disordered regions. However, detailed experimental interrogation is required to determine how individual sequence features, such as SLiMs, underlie higher-order assemblies and mediate distinct molecular activities.

Experimental mapping of the relationship between protein sequence and function is challenging when that function involves a collection of molecular activities (*17*). To date, systematic exploration of protein sequence-function relationships has focused on mutation scanning experiments in which functional output is compared for a library of mutants spanning the length of the protein. This approach has been limited to activities linked to easily tracked cellular phenotypes, such as proliferation or abundance of a single molecular feature, which facilitate the selection of a population of cells (*18*–*22*). Alternatively, bulk genomic measurements capture more holistic phenotypes; however, throughput and cost associated with these approaches substantially reduce the scale of mutants that can be queried (*23*).

Pooled, perturbation-indexed single-cell assays can bridge the gap between traditional genetic screens and low-throughput, information-rich assays (*24*–*26*). Cells genetically modified in a large pool can be analyzed to link perturbations to their effects on complex molecular phenotypes and single-cell heterogeneity. Perturb-seq (*24*) is a method to link genetic alterations to transcriptomic phenotypes. Similar in experimental design, Spear-ATAC (assay for transposase-accessible chromatin) (*27*) measures global chromatin accessibility along with a genetic modification barcode in cells enabling associations between genetic perturbations and transcription factor activity. Similar methods have been employed to explore gene disruption, gene activation, and genetic variation at the epigenomic, transcriptomic, and protein level (*27*–*31*). We sought to extend this general approach to the problem of systematic protein sequence-function mapping.

We developed a pooled screening workflow to assign each region of LAT to its function in T cell activation. Capturing the widespread molecular activities associated with LAT function, we measured epigenome, transcriptome, and surface protein dynamics in single cells expressing a large collection of LAT mutants.

Results

A pooled screen links protein sequence to high-content readouts of parallel LAT activities

We designed a library of open reading frames (ORFs) to interrogate the sequence-function relationship of LAT (Fig. 1B). These ORFs consisted of a mutation scan in which sequential sets of three amino acids were mutated to alanine, as well as a series of negative controls expressing green fluorescent protein (GFP), mutants suggested by previous studies, and missense mutations observed in humans (data S1). We engineered complementary DNA (cDNAs) encoding each ORF, along with an ORF-specific 14-bp (base pair) barcode with adjacent Perturb-seq (*28*) and Spear-ATAC (*27*) primer binding sites in the 3′ untranslated region (UTR), in a lentiviral expression vector (fig. S1A and data S2). We generated lentivirus in an arrayed fashion from each construct and independently titered and pooled them for equal representation (Fig. 1C and materials and methods).

To evaluate the ability of these open reading frames (ORFs) to restore LAT function in T cell activation, we used CRISPR-Cas9 to delete LAT in Jurkat T cells and isolated a clone with dual-allele frameshift indels (fig. S1B and materials and methods). Upon reintroduction of wild-type (WT) LAT, these cells exhibited the expected chromatin and gene expression responses to TCR stimulation, similar to those observed in primary human T cells (fig. S1, C and D). We transduced the Jurkat LAT knockout (KO) cell line with the 132 ORF library lentiviral pool, selected for transduced cells, stimulated the TCR with anti-CD3 antibody, and performed single-cell chromatin accessibility sequencing

[1]Broad Institute of MIT and Harvard, Cambridge, MA, USA. [2]Institute for Medical Engineering & Science, Department of Chemistry, and Koch Institute for Integrative Cancer Research, Massachusetts Institute of Technology, Cambridge, MA, USA. [3]Ragon Institute of MIT, MGH, and Harvard, Cambridge, MA, USA. [4]Department of Biological Engineering, Massachusetts Institute of Technology, Cambridge, MA, USA. [5]Department of Chemistry, University of California, Berkeley, CA, USA. [6]Department of Biology, Massachusetts Institute of Technology, Cambridge, MA, USA. ***Corresponding author. Email: adam@broadinstitute.org (A.J.R.); aviv.regev.sc@gmail.com (A.R.); shalek@mit.edu (A.K.S.)** †These authors contributed equally to this work. ‡These authors contributed equally to this work. ¶Present address: Genentech, South San Francisco, CA, USA.

Downloaded from https://www.science.org at Broad Institute on April 30, 2026

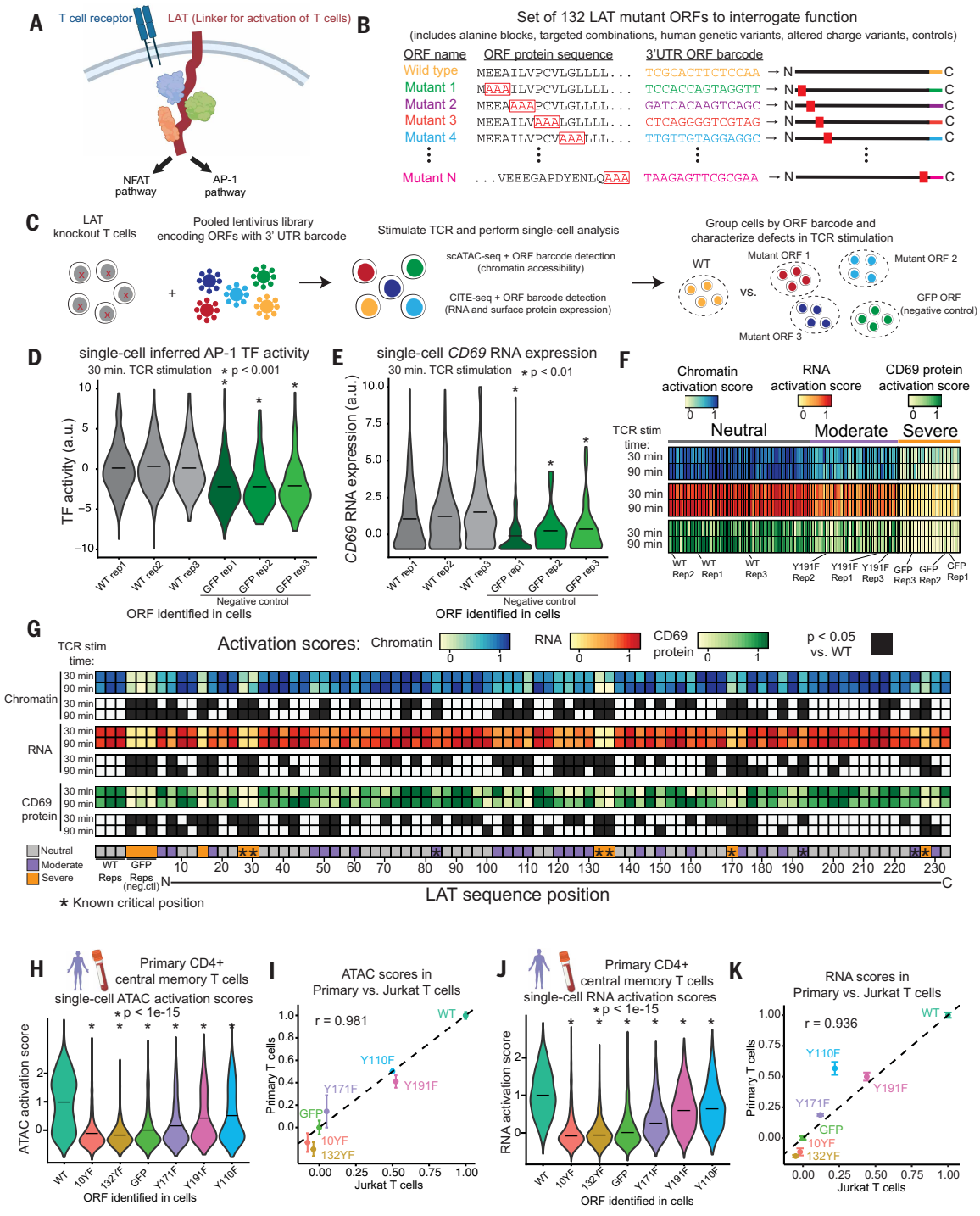

Fig. 1. A pooled screen links protein sequence to high-content readouts of parallel LAT activities. (**A**) LAT is a largely disordered membrane-integrated adapter protein which, upon TCR stimulation, aggregates numerous protein interactors to trigger intracellular signaling pathways. (**B**) Triple alanine block mutant ORFs were designed to cover the entire length of LAT. Other ORFs in the library include single and multisite mutants reported in previous studies, variants observed in humans, ORFs altering net charge, and controls. Each ORF is encoded in a cDNA expression construct with an ORF-identifying barcode in the 3′ UTR. (**C**) A single pool of lentivirus corresponding to all 132 ORFs was used to transduce LAT-knockout Jurkat T cells for subsequent TCR stimulation and single-cell epigenomic, transcriptomic, and protein characterization. (**D**) Violin plot of mean inferred AP-1 transcription factor activity from chromatin accessibility for cells assigned to one of the WT or GFP (negative control) replicate ORF barcodes at 30 minutes of TCR stimulation. Replicate ORFs are identical except for the barcode. Values derived from chromVAR z-scores computed in Signac. *P* value from cell sampling test (materials and methods). (**E**) Similar to (D), for RNA gene expression of *CD69* from the 30-minute TCR stimulation CITE-seq experiment. Values derived from single-cell transform (SCT) residuals computed in Seurat. (**F**) Heatmap of ORF activation scores (mean scores across cells), clustered by k-means. Scores are scaled such that 0 represents the mean of GFP (negative control)–expressing cells and 1 represents the mean of WT LAT–expressing cells. (**G**) Heatmaps representing chromatin, RNA, and CD69 protein activation scores for ORFs encoding alanine blocks. Scores with $P < 0.05$ are shaded black in corresponding heatmap rows, and known critical positions are marked with an asterisk. Neutral, moderate, and severe indicate cluster labels. (**H**) Violin plot of chromatin activation scores for primary human $CD4^+$ central memory T cells assigned to each ORF. Scores are scaled such that the mean score of WT LAT-expressing cells equals 1 and the mean score of GFP-expressing cells equals 0. *P* value from the Kolmogorov–Smirnov (KS) test. (**I**)

Downloaded from https://www.science.org at Broad Institute on April 30, 2026

Scatterplot comparing chromatin activation scores between Jurkat T cell and primary human T cell models. Scores represent the mean of values across two biological replicate stimulation samples, and the value for each replicate was derived from the mean across cells expressing a particular ORF in that replicate. Error bars represent standard deviation across samples. r indicates Pearson correlation. (**J**) Similar to (H) for RNA activation score. (**K**) Similar to (I) for RNA activation score. a.u. indicates arbitrary units from chromVAR z-scores or SCTransform residuals. For all single-cell data, cell numbers for each group are included in data S4.

[scATAC-seq, with Spear-ATAC (*27*) modifications for ORF barcode recovery] or single-cell RNA (scRNA) plus protein [cellular indexing of transcriptomes and epitopes by sequencing (CITE-seq)] (*32*), with Perturb-seq (*28*) modifications for ORF barcode recovery) profiling using the 10x Genomics platform. CITE-seq enabled detection of surface expression of the protein cluster of differentiation 69 (CD69), a canonical marker of T cell activation. We analyzed cells stimulated for 30 or 90 min to capture events associated with early signaling and maximal activity of the AP-1 pathway (fig. S1E). Analysis of the ORF barcodes indicated that individual cells generally express a single dominant ORF (fig. S1F). After filtering for cells with high-quality scATAC and scRNA features and confident single ORF barcode identification, we retained 20,558 cells for the 30-min stimulation and 25,734 cells for the 90-min stimulation in the scATAC experiment and 20,274 and 22,202 cells in the matched CITE-seq experiments (fig. S1G). This corresponded to a mean of 152 to 193 cells per ORF in each experiment (fig. S1H), substantially exceeding the ~50 cells per perturbation that previous power analyses suggested are sufficient for robust phenotyping of knockout (*24*) or coding variant (*28*) effects. Together, these workflows yielded data to link single-cell chromatin accessibility, RNA, and surface protein expression to specific ORF barcodes.

As an exploration of the ability of these data to inform ORF function, we compared groups of cells expressing WT LAT, known functional mutants of LAT, and GFP. Individual accessible chromatin sites, inferred transcription factor (TF) activity, the expression of single or groups of RNAs associated with T cell activation, and CD69 surface protein levels were reduced in cells expressing mutant LAT or GFP versus WT LAT (Fig. 1, D and E, fig. S2, A and B, and data S3) (*1*, *33*). These results indicated that our pooled single-cell ORF screen distinguished defective and functional restoration of TCR signaling, supporting interrogation of the 132-ORF variant library.

In principle, there are two major ways to assess variant effects based on a high-dimensional profile (*34*): One uses the full profile or all relevant features together as a variant impact score (*28*), and the other decomposes the profile to identify the impact on different pathways, genes, or programs (*24*). We pursued each approach in turn.

To summarize the high dimensional chromatin and RNA data, we established a score distinguishing cells expressing WT LAT and GFP in TCR stimulation (materials and methods). Unsupervised feature selection did not reliably distinguish normal and perturbed cells (fig. S2C), so we developed a score by which each cell is assessed across the average of the top 50 respective features (TF motifs for chromatin, genes for RNA), and these values are further averaged across all the cells sharing one ORF. These chromatin and RNA scores, as well as CD69 protein levels, were then scaled such that 0 represents the mean level in GFP-expressing cells and 1 represents the mean level in WT LAT-expressing cells (data S4 and materials and methods). Using these scaled scores, we performed k-means clustering and identified three groups of ORFs (Fig. 1F and fig. S3A). The first cluster contained all three WT LAT replicates and 61 other ORFs exhibiting generally neutral effects on activation. A second cluster, containing all three replicates of Y191F [mutation of tyrosine at position 191 to phenylalanine, known to disrupt a protein interaction motif (*5*, *35*)] and 37 other ORFs, showed moderate loss of activation. The most severely defective ORFs fell into a third cluster, which contained all three GFP replicates as well as 25 other ORFs. These data supported the reproducibility and extent of defects observed in the screen.

Mutations may influence protein expression levels. This defect could challenge interpreting the effect of mutations on molecular activities such as protein interactions or trafficking (*17*). To address this possibility, we performed a modified version of the inCITE-seq experiment to enable the detection of protein epitopes within cells through DNA oligo-conjugated antibodies (*36*). We used an anti-FLAG CITE-seq antibody targeting the N terminus of each ORF to quantify protein expression (fig. S3B). Overall protein expression was not related to a combined chromatin and RNA activation score ($P = 0.337$), indicating that our results likely reflected altered molecular activities of LAT rather than alterations in abundance.

To understand the distribution of functional sequence throughout LAT, we examined the activation scores for each ORF in the mutation scan in linear order (Fig. 1G). We estimated the probability that a given ORF altered a score by chance by randomly sampling single cells from the pool of cells expressing WT LAT, thereby incorporating cell number and heterogeneity to establish statistical power (fig. S3C and materials and methods). Mutants spanning known critical residues exhibited strong defects across each modality, including: cysteines 26 and 29, which are palmitoylated and required for membrane localization (*37*); tyrosine 132 (Y132), which is phosphorylated and serves as a docking site for phospholipase C gamma 1 (PLCG1) (*5*, *35*); and Y171, Y191, and Y226, which are also phosphorylated and bind other adapter proteins including growth factor receptor-bound protein 2 (GRB2) (*2*, *5*, *35*). Additional defects included the proline-rich stretch of PIPRSP (residues 80 to 85), which binds the SH3 domain of LCK to promote ZAP70 localization to LAT (*8*). These expected defects indicated that our experiment captured known biology and allowed for exploration across LAT.

Beyond these known regions, more than 40% of mutant scan blocks fell into the moderate or severe clusters. Out of 32 alanine blocks exhibiting function, 10 were strictly associated with no prior functional evidence (data S4). To validate the function of previously uncharacterized sites, we selected eight positions, separately transduced cells with the corresponding individual mutant ORFs, stimulated them with anti-CD3 antibody, and performed flow cytometry analysis for CD69 surface protein expression (fig. S4, A and B). These mutants all conferred activation defects, thus confirming that our approach can identify functional sites within LAT.

To extend our results beyond the Jurkat T cell model, we asked whether similar mutant ORF phenotypes manifested in primary human CD4+ memory T cells. We knocked out endogenous LAT in primary T cells, delivered six LAT variants and GFP, pooled cells, and performed scATAC-seq and scRNA-seq with ORF barcode detection. After distinguishing central and effector memory T cell states using canonical marker genes, we scored each cell for chromatin and RNA activation and found that LAT variants recapitulated defects at a similar severity observed in the Jurkat T cell screen (Fig. 1, H and K, and fig. S4C). We performed a similar experiment to investigate the function of the eight previously uncharacterized sites in primary human T cells and found that six conferred defects, potentially suggesting context-specific posttranslational modification at phosphorylation or protein interaction sites (fig. S4D). Together, these results indicated that our high-content screen recovered known functional sites in LAT and discovered other sites with relevance in primary human T cell activation.

Determinants of sequence function in LAT

We sought to map sequence features underlying function in LAT comprehensively. Beginning with sequence conservation, we used the ConSurf tool to score each alanine block by mean conservation score and found, as expected, that known critical residues such as cysteines 26 and 29 and tyrosines 132 and 171 resided in highly conserved blocks (Fig. 2A) (*38*).

Downloaded from https://www.science.org at Broad Institute on April 30, 2026

Mutants from the severe cluster were highly conserved ($P < 1x10^{-3}$ in comparison to neutral cluster mutants using a combined chromatin and RNA score) (fig. S5, A and B). Although moderate cluster mutants were more conserved than neutral mutants ($P < 0.05$), both moderate and neutral mutants spanned a broad range of conservation levels, from high to the most poorly conserved positions in LAT.

Conserved sites in disordered proteins often harbor short motifs controlling interaction with other proteins, posttranslational modification, or subcellular trafficking (*11*). To characterize these regions, we used the eukaryotic linear motif (ELM) database, which identified motifs throughout LAT, mostly in the ligand-binding and posttranslational modification categories (Fig. 2B and data S5) (*12*). This analysis identified

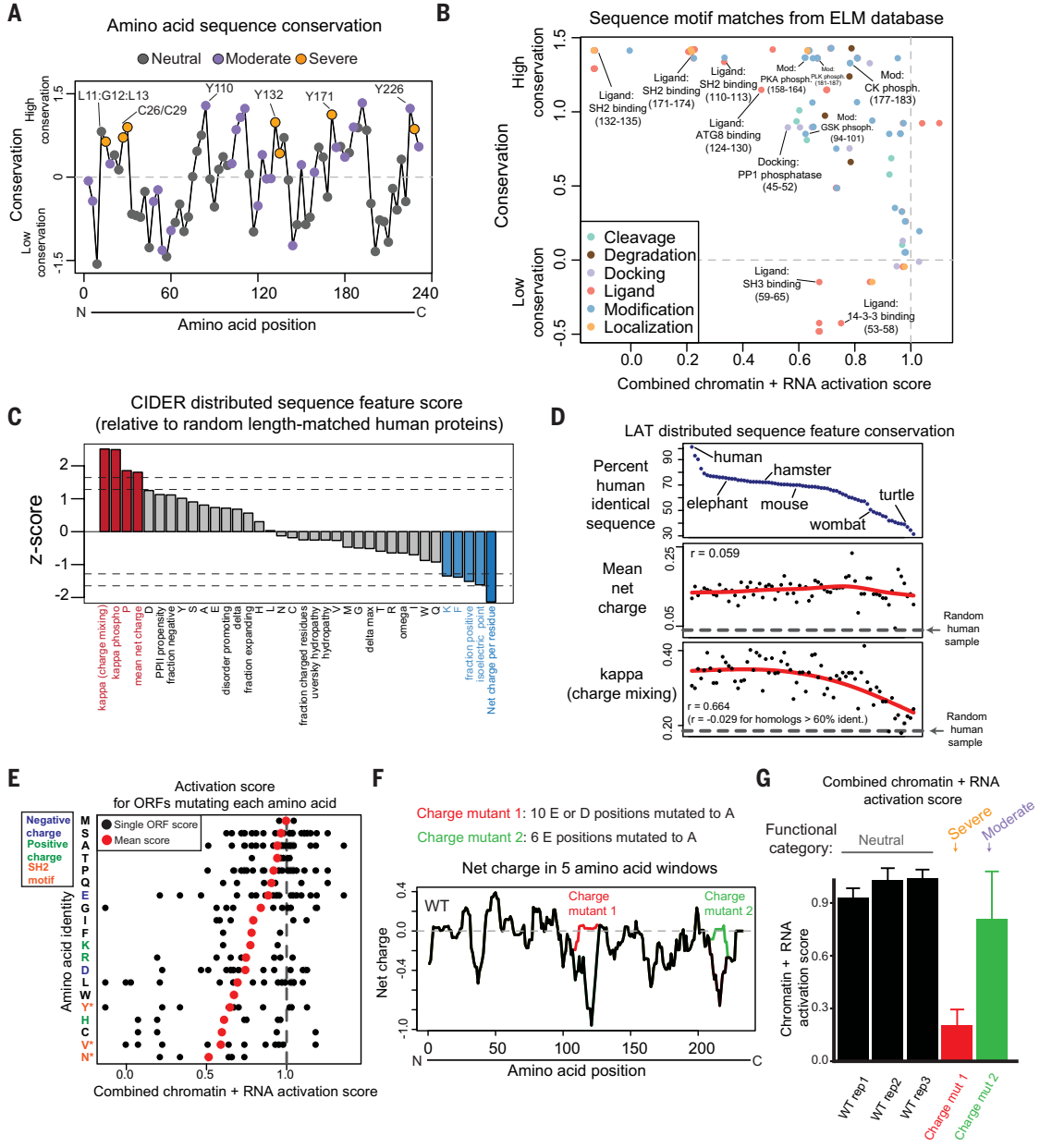

Fig. 2. Discrete and distributed sequence features control LAT function. (**A**) Amino acid sequence conservation of triple alanine blocks was calculated using the ConSurf tool (*38*). ConSurf computes a normalized score for each residue in the protein, whereby the mean value across all residues is 0 and the standard deviation is 1. Plotted values represent the mean conservation score for residues in the three-residue block. (**B**) Scatterplot of combined activation score (from chromatin and RNA scores at 30 min and 90 min stimulation time points) versus conservation for each motif instance discovered using the eukaryotic linear motif (ELM) database. (**C**) Bar plot indicating the z-score of various sequence features for LAT compared with 100 random length-matched human proteins. Feature values were computed by localCIDER (materials and methods). Vertical lines at 5 and 10 percentiles. (**D**) Scatterplots of localCIDER distributed amino acid sequence features for LAT orthologs, ordered by amino acid sequence identity with human LAT. Pearson correlation (r) calculated between sequence identity percent and each feature. The red line indicates a smooth spline calculated in R and gray line represents the mean of random length-matched human proteins. (**E**) For each amino acid, dots represent each ORF in which that amino acid is mutated at least once, and location on the *x*-axis indicates the combined activation score for that ORF. A red dot indicates the mean across all ORFs mutating a particular amino acid. Asterisk indicates $P < 0.05$ compared with mean of score for all residues based on permuting residue positions. (**F**) Running charge (mean within five amino acid windows) for WT LAT and charge mutants. (**G**) Combined activation scores for each charge mutant with labels for functional category. Error bars represent standard deviation across four separate measures composing the combined activation score (chromatin and RNA scores at 30 min and 90 min stimulation time points) (data S4).

Downloaded from https://www.science.org at Broad Institute on April 30, 2026

previously characterized tyrosine-containing Src homology 2 (SH2) domain-binding motifs that had severe phenotypes and were highly conserved. In addition to tyrosine motifs, we found motif matches that potentially explained the function of several sites that are moderately conserved and associated with moderate phenotypes, involving phosphorylation addition or removal and protein interaction. Inspection of multiple sequence alignments indicated that critical residues within these motifs were often near-perfectly conserved across distant orthologs (fig. S5C). Additional, apparently poorly conserved yet functional, motif matches (14-3-3 protein and SH3 domain ligands) contained a mix of highly conserved and poorly conserved residues. This pattern may reflect how flexible sequence grammar is compatible with disordered protein regions.

Beyond short sequence motifs, disordered proteins exhibit conserved biophysical features, determined by their total sequence, which are critical for function and may be maintained through evolution independently of primary sequence (*39*–*42*). To nominate such features with potential roles in LAT, we used the classification of intrinsically disordered ensemble regions (CIDER) tool (materials and methods) (*43*). Several features were distinct from random length-matched human proteins, such as charge mixing, mean net charge per residue, fraction of positively charged residues, proline content, and phenylalanine content (Fig. 2C). Further supporting the importance of these features, mean net charge per residue was conserved across orthologs, extending to ~30% sequence identity, whereas charge mixing (a measure of blocks of charge) was conserved across orthologs down to ~60% sequence identity (Fig. 2D). Multiple sequence alignments for LAT orthologs at the charge blocks suggested that charge is maintained even while exact sequence identity is altered through mutations to residues with similar charge or insertions of charged residues (fig. S5C). The high fraction of disorder promoting residues and low fraction of positively charged residues were also conserved (fig. S6, A and B). These measures highlighted the extent and distribution of negative charge as important features of LAT, consistent with a previous study of in vitro reconstituted signaling (*44*).

To understand the functional consequences of amino acid biophysical features in LAT, we calculated the average activation score for alanine blocks mutating each amino acid (Fig. 2E). Tyrosine (Y), valine (V), and asparagine (N) were the only defective residues ($P < 0.05$ for each), consistent with their repeated occurrence in LAT's well-characterized SH2 domain binding sites (*45*). Mutating individual instances of charged residues, however, did not generally alter LAT function, further suggesting that the total extent and distribution of charge may be important. To investigate this possibility, we examined two ORFs designed to considerably alter regions of concentrated negative charge (Fig. 2F). Charge mutant one (ORF ID 110) converted 10 proximal E or D positions to neutral residues, whereas charge mutant two (ORF ID 111) similarly converted six residues, resulting in an increased net charge from −28.9 to −18.9 and −22.9, respectively. Charge mutant one resulted in consistent defects ($P < 0.05$ in at least one time point in all three modalities) and was in the severe cluster, whereas charge mutant two exhibited a more moderate effect (Fig. 2G). Consistent with previous findings, these results indicated that the total extent, and likely the linear patterning, of negative charge along LAT are critical features (*46*).

We concluded that while conservation is a feature of the most critical regions, more moderately functional regions may exhibit a range of evolutionary or contextual roles. Further, the distributed biophysical sequence feature of charge patterning supported a mechanism independent of local sequence identity which may involve partitioning of LAT-interacting proteins based on charge (*44*) or maintaining an extended chain to prevent intramolecular cross-links that would compete with intermolecular cross-links underlying the formation of a higher-order assembly (*47*, *48*).

Functional interpretation of natural human genetic variants

We reasoned that our experiment could also inform the interpretation of human genetic coding variants. To this end, we included in our library four missense mutations reported in ClinVar, a database of potentially clinically relevant variants (*49*). None of these variants had been experimentally evaluated, and their predicted functional impacts from tools summarized in VarSome [including Sorting Intolerant from Tolerant (SIFT), Protein Variation Effect Analyzer (PROVEAN), and PrimateAI-3D] ranged from likely benign to pathogenic (*50*). These prediction tools primarily leverage sequence conservation and are thus a poor match for disordered regions that often maintain function independent of sequence. In our data, three of the four ClinVar variants (P59A, P82L, and P141L) conferred modest yet statistically significant differences in activation compared with WT LAT (fig. S6C). We extended these findings by leveraging overlapping alanine block scan mutants to examine potential functions of all missense variants in LAT observed at least twice in humans in the Genome Aggregation Database (gnomAD) (fig. S6D) (*51*). The block corresponding to V7F, which was found at the second highest allele frequency (8×10^{-4}) and in two individuals as homozygous, was in the moderate defect cluster (combined activation score 0.58, $P < 0.05$ across all modalities and time points). To understand the impact of the precise genetic variants nominated in this analysis (beyond the associated triple-alanine block mutants), we delivered the exact sequences encoding four potentially functional variants from the gnomAD database to primary human CD4+ T cells (fig. S6E). Variants encoding V7F (likely through disruption of the transmembrane domain) and E111K (likely through loss of a highly conserved negatively charged residue involved in tyrosine phosphorylation at position 110) altered activation (fig. S6F). The variant P59A did not alter activation, possibly due to the redundant function of neighboring proline residues serving as a noncanonical SH3 ligand. The other nonfunctional variant, V134M, appeared to alter a residue that is poorly conserved and even tolerant to an alteration in charge (whereas the corresponding triple-alanine block disrupted highly conserved residues forming the SH2 binding ligand at Y132). Overall, our data reinforced the potential for mutation scanning with focused confirmation experiments to inform functional interpretation of human genetic variants.

LAT encodes downstream pathway balance

We next sought to understand whether individual functional sites in LAT related to one or more distinct signaling pathways. LAT could trigger downstream pathways in a modular fashion, by which molecular events at distinct regions of LAT are independent and contribute to distinct pathway outputs, or in a coordinated fashion, by which LAT must form a fully functional signalosome to trigger activation of any and all downstream pathways (Fig. 3A). We hypothesized that analyzing how mutants affect the activities of individual TFs associated with particular pathways would enable mapping LAT sites to pathways and provide support for either a modular or coordinated model (Fig. 3B). In a modular model, mutants may affect one pathway yet not necessarily affect others; in the coordinated model, any mutant affecting one pathway will correspondingly affect other pathways.

With these models in mind, we compared inferred TF activities from chromatin accessibility data of the AP-1 family member FBJ osteosarcoma oncogene (FOS) and the NFAT family member nuclear factor of activated T cells 1 (NFATC1), representing two of the critical pathways engaged in T cell activation (Fig. 3C and materials and methods). We observed a linear relationship between the two inferred TF activities, whereby mutants disrupting AP-1 activity consistently disrupted NFAT activity to a similar extent. Overall, 36 mutants were coordinated (conferring comparable defects in both pathways). One mutant exhibited a biased defect, potentially mediated through the disruption of posttranslational modification or ligand binding sites (fig. S7A). Consistent with the observed defect in NFAT signaling with maintained AP-1 signaling, the gene expression defects for the biased mutant did not include AP-1 family genes themselves which are autoregulated by AP-1 TFs (*52*) (fig. S7, B and C). Mutants conferring coordinated defects in

Downloaded from https://www.science.org at Broad Institute on April 30, 2026

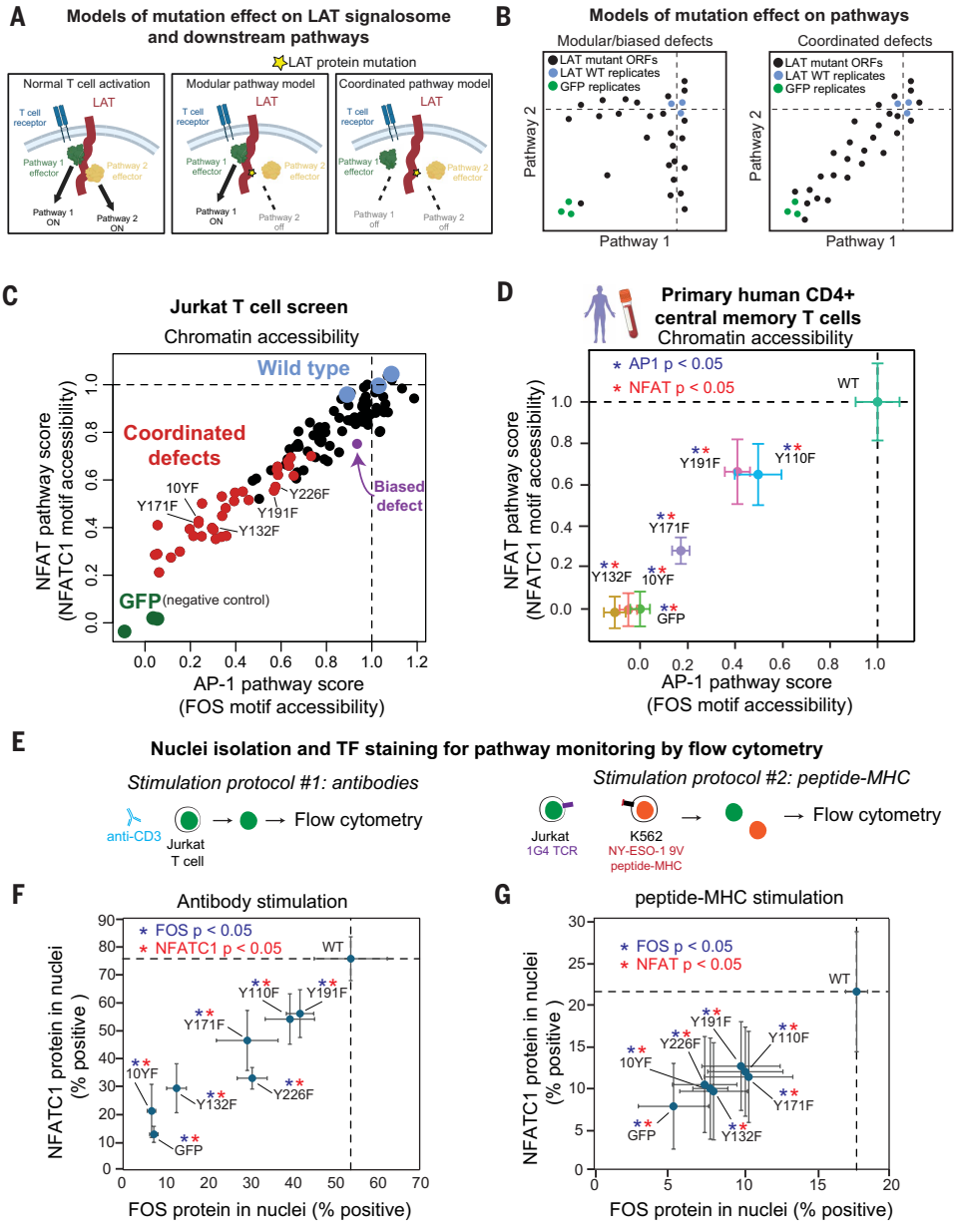

Fig. 3. LAT encodes downstream pathway balance. (**A**) Models of LAT with interacting proteins which mediate intracellular signaling pathways. The complex of LAT with interactors ("signalosome") could control downstream pathways in a modular or coordinated fashion. In a modular model, mutation in one region of LAT and disruption of a particular interactor will disrupt one downstream pathway while leaving others active. In a coordinated model, mutation in one region of LAT which disrupts a particular interactor may disrupt other interactions or pathway activities (potentially through higher-order physical assembly). (**B**) Expected results for the models proposed in (A). Modular or coordinated signaling will exhibit distinct patterns of mutant effects on pairs of pathway activities measured in the screen. (**C**) Scatterplot of the accessibility of two chromatin features (inferred TF activity, averaged across cells expressing a particular ORF) representing central pathways of T cell activation. *P* value from permutation sampling test. ORFs supported by at least 40 cells are displayed. Coordinated defects exhibit statistically significant defects in both AP-1 and NFAT pathways. One mutant represented as a purple dot exhibited a defect in the NFAT pathway only. (**D**) Scatterplot of AP-1 and NFAT TF activity in primary human CD4+ central memory T cells. Error bars represent standard deviation across two biological replicates, *P* value from KS test of single-cell values. Cell numbers for each group are noted in data S4. (**E**) Schematic of two experimental designs to measure the impact of TCR stimulation on pathway activation through flow cytometry. The abundance of TFs in the nucleus was measured in isolated nuclei by staining for FOS or NFATC1 proteins. Jurkat T cells were stimulated using anti-CD3 antibodies or through the delivery of the 1G4 TCR and coculture with K562 cells expressing 1G4-cognate NY-ESO-1 9V peptide on major histocompatibility complex class I (MHCI). (**F**) Scatterplot of flow cytometry results (percent positive nuclei) for antibody-stimulated LAT KO Jurkat T cells expressing one of indicated ORFs. Error bars represent the standard deviation of measurements from three biological replicate stimulations. (**G**) Similar to (F), for cells stimulated through peptide-MHC. Error bars represent the standard deviation of measurements

the Jurkat T cell screen all had defects in both AP-1 and NFAT pathways in primary human CD4+ central memory T cells (Fig. 3D).

To extend these findings, we implemented an orthogonal experimental approach to measure the impact of LAT mutation on pathway activation at the protein level. After isolating the nuclei of T cells undergoing TCR stimulation, we measured TF translocation to the nucleus by immunostaining for individual TFs and performing flow cytometry (*33*) (Fig. 3E and fig. S8, A to C). In Jurkat T cells expressing WT LAT and stimulated with anti-CD3 antibody, TFs FOS and NFATC1, responsive to AP-1 and NFAT pathway signaling, respectively, demonstrated nuclear abundance with kinetics similar to that of inferred TF activity from chromatin accessibility (fig. S8D). By delivering mutants conferring coordinated defects in the screen, we found that pathway activation again appeared coordinated after 1 hour of stimulation: Mutants that disrupted the nuclear abundance of FOS also disrupted the nuclear abundance of NFATC1 (Fig. 3F). Subtle differences in signal initiation have been shown to trigger distinct pathway activity at later time points (*53*). We therefore repeated the stimulation for 12 hours but found that pathway defects were similar to the results observed at the 1-hour time point (fig. S8E). As a separate measure of AP-1 pathway activity, we also stained cells for phosphorylated extracellular signal-regulated kinase (ERK) after TCR stimulation. Similar to the measurement of nuclear FOS, all examined mutants conferred a defect in phosphorylated ERK, reinforcing the notion that LAT mutation alters early signaling events (fig. S9, A and B).

We also considered the possibility that TCR stimulation through anti-CD3 antibody-induced cross-linking initiates an overly powerful response that is not representative of physiological interactions between T cells and peptide major histocompatibility complex (MHC)–expressing cells. To understand whether LAT mutation conferred coordinated defects in a system relying on TCR engagement with peptide-MHC, we delivered the human-derived 1G4 TCR to Jurkat T cells, incubated them with dye-labeled K562 cells expressing cognate peptide-MHC from the cancer antigen NY-ESO-1, and detected pathway activation in isolated nuclei by flow cytometry (*54*, *55*) (Fig. 3E). Stimulation of Jurkat T cells expressing WT LAT by coculture with K562 cells induced similar kinetics to antibody stimulation and was dependent on cognate peptide-MHC expression on K562 cells (fig. S9C). Similar to stimulation with

Downloaded from https://www.science.org at Broad Institute on April 30, 2026

from four biological replicate stimulations. For flow cytometry experiments, *P* values derived from two-tailed *t*-test and cells were gated as in fig. S8B with the addition of a CellTrace Yellow-negative gate for the coculture experiment.

the anti-CD3 antibody, mutants that disrupted the nuclear abundance of FOS also disrupted the nuclear abundance of NFATC1, indicating that LAT mutations confer coordinated defects in pathway activation in the context of physiological T cell activation (Fig. 3G). We observed similar results using antigen-presenting cells pulsed with peptide variants representing a range of TCR–peptide-MHC (pMHC) affinities (fig. S9D).

We next sought to understand how LAT mutation affected pathways beyond AP-1 and NFAT. We found that TFs representing other families induced in T cell activation exhibited similar overall trends in coordinated activity (fig. S10A). Upon closer examination of TF activity decoupling, we observed numerous ORFs exhibiting moderate biased defects (fig. S10B). These biased ORFs tended to be moderate in their effect size, potentially indicating that signaling responses beyond the major pathways of AP-1 and NFAT were more sensitive to subtle alterations in the strength or biased signal initiation at LAT. To further explore modularity in this expanded set of TFs, we examined chromatin accessibility at individual stimulation-dependent genomic regions containing each associated TF motif (fig. S10C). We observed a generally uniform trend of accessibility loss across regions. Closer interrogation of the distributions of accessibility across genomic regions suggested that a subset of regions is altered substantially in addition to a broad shift in accessibility for larger set of regions (fig. S10D).

As a final aspect of potential signaling modularity, we interrogated whether analysis of individual genes (rather than pathways or programs) revealed sets of mutant-specific, coregulated features. We failed to identify distinct clusters; indeed, it appeared that stimulation-dependent genes were affected uniformly by alterations in LAT signaling (fig. S11, A and B).

We concluded that LAT mutations generally conferred coordinated defects across multiple downstream pathways. Mutants disrupting one pathway consistently disrupted other pathways to a similar extent, thus maintaining a balance in the relative levels of signaling pathways.

Indirect disruption of protein interactions underlies balanced defects

We sought a molecular explanation for how initiation of multiple signaling pathways from LAT could be sensitive to the disruption of any individual segment. We reasoned that defects may be conferred through disruption of direct binding proteins and thus set out to comprehensively map which proteins may directly bind LAT and at which sites. Starting from a list of 10 LAT interacting proteins identified in an affinity purification mass spectrometry (ms) dataset, we used AlphaFold-Multimer to predict interaction structures and nominate sites of direct binding (*56*, *57*). Of the 10 proteins, four had AlphaFold-Multimer support as direct binders to segments of the disordered cytoplasmic tail of LAT: PLCG1, GRB2, GRB2-related adaptor downstream of Shc (GADS), and GRB2-related adaptor protein (GRAP) (fig. S12A). Each of these proteins contains phospho-tyrosine binding SH2 domains and have some evidence for binding a subset of LAT tyrosines (*6*, *58*). To determine which LAT tyrosines bind which of these proteins, we re-ran AlphaFold-Multimer with LAT and the isolated SH2 domains, and scored each predicted structure based on proximity of the SH2 domain to a single LAT tyrosine (materials and methods). While PLCG1 was predicted to bind LAT position 132 exclusively, GRB2, GADS, and GRAP were predicted to promiscuously bind at any of positions 110, 171, 191, and 226 (Fig. 4, A and B, and fig. S12, B to E). These results were generally consistent with previous studies of LAT tyrosine mutation in cells and through in vitro binding of isolated effector proteins with peptides derived from LAT (*35*, *58*).

One possible explanation for multipathway, coordinated defects from mutating one site on LAT is that loss of protein binders from the mutated site also leads to loss of the binding of other proteins from distant sites, for example because signalosome formation is an all-or-none scenario. Even if the proteins binding each site trigger distinct downstream pathways, a defect in one site would be functionally similar to a defect in another site. Given the established role of PLCG1 phospholipase enzymatic activity mediating NFAT pathway activation and GRB2 as an adapter recruiting son of sevenless (SOS), the critical guanine nucleotide exchange factor for Ras controlling mitogen-activated protein kinase (MAPK) and AP-1 signaling, we sought to explore how these proteins, which appear to bind mutually exclusive sites on LAT, may be functionally linked.

We developed a biotin labeling experiment to quantitatively assess LAT interactor proximity in living T cells. Using TurboID fused to the C-terminus of LAT, we reproducibly and selectively detected PLCG1 and GRB2 interaction with LAT in an activation-dependent manner (Fig. 4C and fig. S13, A and B). As expected, the LAT 10YF mutant (converting all 10 tyrosine residues to phenylalanine) impaired LAT interaction with either PLCG1 or GRB2. Similarly, as expected from previous studies and our AlphaFold modeling, LAT Y132F phenocopied 10YF loss of PLCG1 interaction, indicating that Y132 is the single binding site for PLCG1 (Fig. 4, D and E). Mutations of Y171 and Y191 also conferred PLCG1 loss, potentially through disrupting interaction with GRB2 or GADS, which stabilizes the LAT-PLCG1 interaction through the adapter SLP-76 (*35*). Although mutation of the expected GRB2 binding sites Y171F and Y110F impaired GRB2 interaction, we found that mutation of Y132, the exclusive PLCG1 binding site, also disrupted GRB2 interaction. Previous in vitro studies of GRB2 have shown no detectable binding to Y132 and demonstrated an absolute dependence on asparagine at position +2 relative to the tyrosine, which is absent in Y132 and present at other tyrosine positions analyzed (*58*, *59*).

These results are consistent with a model in which GRB2 and PLCG1 are recruited to the same membrane-proximal condensate through LAT scaffolding. We examined this interaction directly by performing coimmunoprecipitation of GRB2 in T cells and found that PLCG1 co-detection depended on activation and LAT containing both GRB2 and PLCG1 binding sites (Fig. 4F and fig. S13, C and D). Through live-cell total internal reflection fluorescence (TIRF) microscopy of T cells activated by pMHC on supported lipid bilayers, we also observed colocalization of GRB2 and PLCG1 in discrete condensates (Fig. 4G and fig. S14, A and B). A total of 376 PLCG1 condensates were detected, 276 of which exhibited colocalization and a shared growth signal profile with GRB2 (mean 71.2% condensates colocalized across four cells, standard deviation 8.5%) (fig. S14C). This proportion is a lower bound based on the low signal-background ratio (~1.5×) in the GRB2 imaging. Together, our results supported a model in which mutation of a single site can disrupt protein binding events, and thus their related signaling pathways, at distinct, distant sites on LAT (Fig. 4H).

Discussion

Mapping the relationship between protein sequence and function is a fundamental problem in biology. Here, we employed a high-content screen to link the amino acid sequence of the adapter protein LAT to its multifaceted function branching TCR stimulation to numerous downstream pathways.

Individual signaling pathways appear coordinated: LAT mutants affecting one pathway generally affect others to a similar extent. This coordination may occur at the LAT signalosome itself as a result of the overlapping roles of interacting proteins as pathway-specific effectors (adapters or enzymes) and cross-linking agents bridging LAT molecules to promote cluster formation at the membrane (*44*, *60*). With SOS as an intermediate or directly, GRB2 and PLCG1 have been shown to promote clustering of phosphorylated LAT, which may provide

Downloaded from https://www.science.org at Broad Institute on April 30, 2026

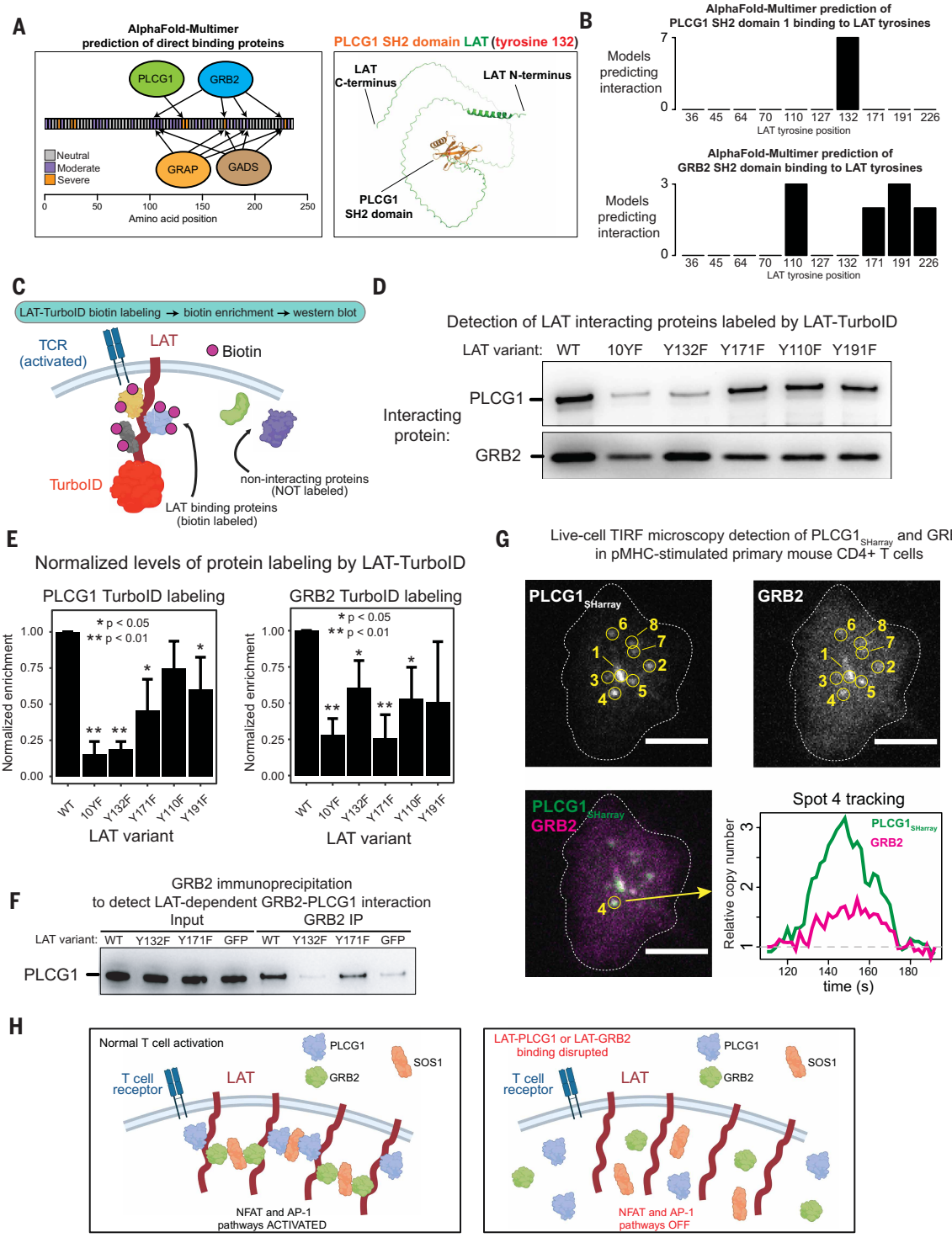

Fig. 4. Indirect disruption of protein interactions underlies balanced defects. (**A**) (Left) Schematic of binding sites of SH2 domains predicted by AlphaFold-Multimer. PLCG1, phospholipase C gamma 1; GRB2, growth factor receptor-bound protein 2; GRAP, GRB2-related adaptor protein; GADS, GRB2-related adaptor downstream of Shc. (Right) Predicted structure of LAT interacting with the PLCG1 N-terminal SH2 domain. (**B**) Counts of models (out of 10 total predicted models) for each LAT interaction with an SH2 domain. Models were scored as interaction with a particular LAT tyrosine based on exclusive proximity of 10 angstroms. (**C**) Schematic of LAT-TurboID proximity labeling experiment. LAT fused to TurboID was expressed in LAT KO Jurkat cells. Cells were activated by pervanadate stimulation for 10 min, and biotinylated proteins were detected by western blot of the streptavidin enriched lysate. (**D**) Representative western blots from four replicate labeling experiments detecting PLCG1 and GRB2 abundance in streptavidin-enriched samples. (**E**) Quantification of band intensity from four replicate labeling experiments. Error bars represent standard deviation and *P* values were calculated by *t*-test. (**F**) Representative western blot from three replicate coimmunoprecipitation experiments. LAT KO Jurkat T cells reconstituted with one of indicated ORFs were stimulated for 5 min with pervanadate before lysis and immunoprecipitation with anti-GRB2-coupled beads. See fig. S13, C and D, for controls and quantification. (**G**) Live-cell TIRF microscopy images of a representative primary mouse CD4+ T cell expressing $PLCG1_{SHarray}$ fused to mNeonGreen and GRB2 fused to mScarlet. Cells are imaged on supported lipid bilayers functionalized with ICAM-1 (100 μm^{-2}) and agonist peptide-MHC (0.1 to 0.6 μm^{-2}); this pMHC ligand density is activating. The numbers

Downloaded from https://www.science.org at Broad Institute on April 30, 2026

identify individual condensates visualized by $PLCG1_{SHarray}$ and corresponding regions in the GRB2 channel. Scale bar, 5 μm. For a single spot, time traces of the relative copy number of $PLCG1_{SHarray}$ and GRB2 show similar growth-dissolution profiles. This shared growth profile was used to score $PLCG1_{SHarray}$ spots as being colocalized with GRB2. Gray line indicates background signal of 1. (**H**) Model of LAT interaction with partner proteins. Disruption of one interaction has indirect effects on distinct interactors, resulting in balanced loss of pathway activation. Uncropped images from western blots are included in fig. S15.

a temporary environment, protected from CD45 phosphatase activity, in which NFAT/Ca^{2+} and MAPK pathways can be initiated (*61*, *62*). Indeed, this environment may promote dwell time of LAT-interacting proteins at the membrane, a highly sensitive factor regulating SOS and other signaling systems (*63*, *64*). Our protein interaction data indicated only partial loss of GRB2 binding to LAT upon mutation of the PLCG1 binding site which may reflect sensitivity of GRB2-recruited SOS to dwell time for activation of Ras and the AP-1 pathway.

These coordinated outputs support a model in which LAT recruits and organizes interaction partners in only one of several molecularly plausible assembly forms (Fig. 4H and fig. S14D). Indeed, LAT assemblies excluding either PLCG1 or GRB2 have been described in vitro (*44*, *60*), yet our data suggest that neither of these configurations, which should have triggered extreme bias in AP-1 versus NFAT pathway initiation, are formed in living cells. This system may constrain the default output of T cell receptor stimulation to avoid the skewed ratio of AP-1 and NFAT pathway activity associated with T cell anergy (*1*). By contrast, a recent study of the Toll-like receptor response found that downstream pathways, although triggered through the recruitment of effector proteins to an adapter assembly in a fashion similar to LAT, were controlled in a modular fashion (*65*).

Our data also likely capture an incomplete picture of the LAT sequence-function relationship as a result of the role of LAT across various T cell developmental stages and states, as well as in natural killer (NK) and mast cells (*66*, *67*). Specific combinations of tyrosine mutants in LAT, which in our data result in similar multipathway defects, have been shown to influence thymocyte development in distinct ways (data S1 and S3) (*35*). High sensitivity to the quantitative levels of signaling pathways in development may explain this discrepancy (*62*). Future experiments in primary T cells of distinct differentiation, memory, or exhaustion states may reveal interactions between LAT and TCR proximal signaling machinery that is differentially expressed or regulated in these states. Cosignaling receptor stimulation may also shift the sequence function map.

Our approach may be extended by capturing further molecular and cellular aspects of T cell activation. Improved CITE-seq methods could monitor intracellular phosphorylation status and protein-protein interactions within the LAT signalosome (*68*, *69*). A hallmark of LAT function is formation of short-lived condensates which could be detected in an optical pooled screen (*70*, *71*). Beyond T cell activation, our approach may be applied to proteins involved in any process that can be monitored at the level of chromatin accessibility, transcriptome, or protein profiling. Our experiment was specifically designed to capture short time points in a stimulation response with the goal of monitoring direct effects of the perturbed protein; this paradigm could extend to proteins involved in processing other immune or development signals.

Recent technologies utilizing sample multiplexing and split-pool cell labeling have made single-cell analysis more cost effective (*72*). Future experiments could maintain cost and increase granularity beyond alanine blocks to single residue mutation or combinatorial mutants to uncover genetic interactions. A major cost reduction, and thus opportunity to increase scale, could come from improvements in the efficiency of base- and prime-editing approaches (*73*, *74*). We employed cDNA delivery by means of lentivirus, requiring individual plasmid cloning and lentiviral production, to ensure that the perturbation barcode detected in our assay in each cell matched the singular genotype present in that cell rather than an unlinked genotype detected through barcode swapping during lentiviral production (*75*). Current mutation efficiencies of ~40% for base- and prime-editing methods would yield a low fidelity of barcodes to genotypes as well. Improvements, however, would unlock a roughly 100-fold decrease in the cost of synthesizing genetic variants upon a switch from plasmid synthesis to single guide RNA synthesis.

Given the similarity of LAT to other adapter-effector signaling systems, interdependent assemblies of interacting proteins may be a general mechanism to constrain signaling outputs in response to extracellular cues. Further, interdependent assembly may extend to disordered protein regions generally, which often function through the role of the IDR as a "scaffold" mediating the recruitment of numerous "client" factors to achieve diverse functions (*76*).

Materials and methods

Generation of LAT knockout Jurkat T cell line

Jurkat Clone E6-1 cells (Jurkats) were purchased (ATCC TIB-152) and cultured in RPMI 1640 (Thermo Fisher 11875093) with 1x Pen/Strep/Glutamine (Thermo Fisher 10378016) and 10% FBS (Life Technologies 10082147). The Cas9-RNP nucleofection protocol from IDT was followed using a separate gRNA and tracrRNA, as well as Cas9 V3 and enhancer oligo products from IDT. The gRNA was designed using the Broad Institute sgRNA Designer tool and selecting the top hit (TTTACCAGTTTGTATCCAAG) which was predicted to create indels in LAT exon 4. The Cas9 RNP complex was generated following IDT's recommendations and transfected into Jurkats using the Neon Electroporation System (Invitrogen). To isolate clones, cells were sorted into wells of a 96 round-bottom plate and left undisturbed in culture for two weeks. Wells with visible growth were resuspended, transferred to fresh media, and expanded. Thirteen clones were subjected to gDNA isolation and Illumina Nextera library preparation to sequence the locus surrounding the expected indel site. Primers LAT_sg2_Nextera_fwd and LAT_sg2_Nextera_rev (data S2) were used to perform PCR as a first stage, followed by an index PCR using Nextera P5 and P7 primers to add Illumina library and index sequences. Libraries were quantified by Qubit, pooled, and sequenced on a MiSeq (single end 130 base read length). The most abundant unique reads were aligned to the LAT locus using Benchling.

Design and synthesis of cDNA library and expression vector

ORFs encoding the alanine block scan, targeted point mutations, GFP, charge alterations, and Cosmic/ClinVar human genetic variants were designed to be expressed in a modified version of the vector p_sc_eVIP (Addgene 168174) (*28*). The 3′ UTR ORF barcode sequence was flanked by ATAC primer binding sites to enable the Spear-ATAC protocol, and a nested primary binding site was added downstream of the barcode to enable a nested PCR in both Spear-ATAC and CITE-seq ORF barcode library generation (fig. S1A). To generate an individual ORF expression vector, we ordered a DNA construct (IDT gBlock or Twist Biosciences Gene Fragment) containing the ORF, primer binding sites neighboring the ORF barcode as described above, and 15 bp homology arms for cloning into p_sc_eVIP digested with NheI. An example construct encoding N-terminal FLAG-tagged LAT is included in data S2, labeled "FLAG-LAT-ORFbc gBlock." This construct contains the following key sequence segments: ATAC Read 1 capture site - TCGTCGGCAGCGTC, ORF barcode – TTCTTCTTCTTCCG, Nested primer binding site 2 – CAGCCCGGGCATTTTGTC, ATAC Read 2 capture site – CCGAGCCCACGAGAC, Nested primer binding site 1 – CAGTCTGAGTCAGGCCCT. The first and last 15 bp compose the homology arms matching the terminal sequences of NheI-digested p_sc_eVIP. Cloning of DNA constructs into the digested p_sc_eVIP plasmid is included in detail in the later materials and

Downloaded from https://www.science.org at Broad Institute on April 30, 2026

methods section describing the generation of the LAT-TurboID fusion expression vector.

For the 132-ORF screen, Twist Biosciences generated the individual expression vectors as a Clonal Genes product and shipped approximately 2-10 ug of each plasmid in separate wells.

Preparation of titered lentivirus pool and transduction of Jurkat KO cells

Lenti-X 293T (HEK) cells (Takara 632180) were cultured in DMEM (Thermo 11995065) with 10% FBS (Thermo Fisher 10082147) and 1x Pen/Strep/Glutamine (Thermo Fisher 10378016). Lentiviral packaging plasmids pMD2.G and pVSV-G were acquired from the Broad Institute Genetic Perturbation Platform. HEK cells were transfected using Lipofectamine 3000 (Thermo Fisher L3000001) following manufacturer's protocol with modifications to achieve a 96-well format. To improve cell adherence, plates were coated with poly-L-lysine (Sigma P8920) for 1 hour at 37°C (0.01% in PBS) followed by three washes with PBS and drying for 30 min at 37°C. HEK cells were seeded at a density of 5.75×10^4 cells per well. The following day, HEK cells were transfected with lentiviral transfer (encoding each ORF) and packaging plasmids. The transfection mix was prepared in a separate 96 well plate by first generating a standard packaging vector mix (10 ul Optimem, 0.33 ul P3000 reagent, 63 ng pVSV-G, 21 ng pMD2.G) and then depositing 83 ng of transfer vector (encoding each ORF) at 10 ng/ul to ensure consistent transfer to each well. A second mix was then deposited into each well containing 10 ul Optimem and 0.42 ul Lipofectamine 3000 and mixed gently by pipetting 7 times. Manipulations were performed using a multi-channel pipet. Complex formation was allowed for 20 min at RT, and then 20 ul of freshly prepared lipid complexes were added directly to HEK culture media.

Media was exchanged after overnight growth. Plates were then cultured for 24 hours for a ~48-hour post-transfection harvest, media was replaced, and a final harvest was taken at 72 hours post-transfection. Harvested lentiviral supernatant was maintained in 96-well format at this stage. An aliquot of each well was taken to perform p24 ELISA (Takara 631476) following manufacturer's instructions on lentiviral supernatant diluted approximately 800-fold. ELISA values were computed to establish a mixing ratio for equal representation of viral particles across all library ORFs, and the ORF-specific lentiviral volumes were pooled for equal representation. The pool was then mixed with Lenti-X concentrator (Takara) following manufacturer's instructions, concentrated, resuspended in PBS, and frozen in aliquots at -80C.

LAT knockout clone Jurkat cells ("Jurkat KO") were transduced by mixing $1/24^{th}$ of the concentrated total viral harvest and 5×10^5 cells in 2 ml media with 8 ug/ml polybrene. After overnight incubation, we performed a media change. At 48 hours post-transduction, cells were resuspended in media containing 0.6 ug/ml puromycin. Cells were cultured for approximately 7-9 days with passaging every 2-3 days to yield a population of viable (>90% by Trypan staining) cells. This amount of virus and transduction format led to roughly 10% transduction efficiency (as measured by proportion of viable cells at 24-48 hours post-selection), suggesting most cells represent a single transduction event.

TCR stimulation, CITE-seq and Spear-ATAC, and library generation

Jurkat KO cells transduced with the lentiviral ORF library pool were harvested and resuspended at 1×10^6 cells/ml in 1ml in a 12-well tissue culture plate to equilibrate for 30-60 min. Cells were then stimulated by adding anti-CD3 (OKT3, Thermo Fisher 16-0037-81, RRID:AB_468854) and anti-IgG (Biolegend 405301, RRID:AB_315005) antibodies at 1 ug/ml for 30 or 90 min before harvesting on ice. Cells were split into separate pools for CITE-seq and Spear-ATAC protocols. For CITE-seq, we followed the BioLegend protocol for simultaneous hashing and antibody staining (http://www.biolegend.com/en-us/protocols/totalseq-a-dual-index-protocol). In brief, cells were blocked and stained with antibodies in Cell Staining Buffer (BioLegend 420201) and TruStain FcX (BioLegend 101319) using 1 ul of each antibody in 100 ul for 30 min followed by three washes in Cell Staining Buffer (data S2). Cells were then counted and cells from the 30-min and 90-min stimulation time points were pooled equally to allow for later distinction by hashing. Cells were loaded onto four channels of a 10x Genomics Chromium Next GEM Chip G at 3×10^4 cells per channel to leverage hash-based identification of doublets with super-loading. For Spear-ATAC, cells underwent nuclei isolation following the 10x Genomics suggested protocol for cell lines. Nuclei were counted and loaded on a 10x Genomics Chromium Next GEM Chip H at a concentration of 3×10^4 nuclei per channel (two channels per time point) to leverage identification of doublets by ORF barcode with super-loading. Following the Spear-ATAC protocol, addition of primer ORF-BC_nested_1_rev (data S2) was included in the encapsulation step and the number of stage one amplification cycles was extended to 15. Hashing (HTO), antibody (ADT), gene expression, and ATAC libraries were generated following 10x Genomics Chromium Next GEM Single Cell 3′ v3.1, BioLegend, and 10x Genomics Chromium Next GEM Single Cell ATAC v1.1 workflows.

ORF barcode library generation from CITE-seq

Note: See data S2 for primer sequences. NEBNext High-Fidelity 2X PCR Master Mix (NEBNext MM, New England BioLabs M0541S) was used for all PCRs. Generation of ORF identifying libraries from the CITE-seq experiment began by performing targeted amplification of the ORF construct from the cDNA material of the 10x Chromium Next GEM Single Cell 3′ v3.1 workflow (Step 2.2).

The first PCR (PCR1) was performed with the following reaction conditions:

Primers: CropDialOut_R1, BC_nested1_rev

Mix: 30ul reaction – 15 ul NEBNext MM, 10 uM each primer, 50 ng cDNA product

Cycling: 98C for 30s; 6 cycles of 98C for 10s, 63C for 15s, 72C for 20s; 72C 1min

This product was purified using 1x SPRIselect beads (Beckman Coulter B23317), with a 15 ul elution in water, and used as input for a second nested PCR (PCR2) with the following reaction conditions:

Primers: CropDialOut_R1, BC_nested_Truseq_R2

Mix: 30ul reaction – 15 ul NEBNext MM, 10 uM each primer, 9 ul PCR1 product

Cycling: 98C for 30s; 6 cycles of 98C for 10s, 63C for 15s, 72C for 20s; 72C 1min

This product was purified using 1x SPRIselect beads, with a 15 ul elution in water, and used as input for a third indexing PCR (PCR3) with the following reaction conditions:

Primers: CropDialOut_P5_R1, P7_Truseq_idx[n]

Mix: 30ul reaction – 15 ul NEBNext MM, 10 uM each primer, 9 ul PCR2 product

Cycling: 98C for 30s; 7 cycles of 98C for 10s, 63C for 15s, 72C for 20s; 72C 1min

This product was purified using 1x SPRIselect beads, with a 20 ul elution in water.

These libraries were quantified by Qubit and Bioanalyzer (to identify the expected 379bp product) before mixing with CITE-seq gene expression, HTO, and ADT libraries for sequencing on a single Illumina NextSeq 2K P3 kit. The following reads per cell were targeted: gene expression – 1.8×10^4, ORF barcode – 1×10^3, ADT – 2.5×10^3, HTO – 1×10^3.

ORF barcode library generation from Spear-ATAC

Note: See data S2 for primer sequences. Generation of ORF identifying libraries from the Spear-ATAC experiment followed the published protocol with modification to the intermediate library purification strategy. Using the scATAC library as input, we performed a PCR (PCR1) using reaction conditions:

Primers: P5_fwd, BC_nested_Truseq_R2

Downloaded from https://www.science.org at Broad Institute on April 30, 2026

Mix: 30ul reaction – 15 ul NEBNext MM, 10 uM each primer, 50 ng scATAC library

Cycling: 98C for 30s; 10 cycles of 98C for 10s, 63C for 15s, 72C for 20s; 72C 1min

This product was separated on a 2% TAE-agarose gel for one hour at 120V. A size range of 100 to 170 bp was excised (to capture the expected 119bp amplified fragment and exclude off-target amplicons), purified with a 22 ul water elution, and used as input for a nested PCR with reaction conditions:

Primers: P5_fwd, P7_Truseq_idx[n]

Mix: 50 ul reaction – 25 ul NEBNext MM, 10 uM each primer, 15 ul purified PCR1

Cycling: 98C for 30s; 7 cycles of 98C for 10s, 63C for 15s, 72C for 20s; 72C for 1 min

This product was then purified using 2x SPRI beads and a 22 ul elution in water. These libraries were quantified with Qubit and Bioanalyzer (to identify the expected 158 bp product) and sequenced on an Illumina MiSeq using a 150-cycle Reagent Kit v3. Custom primer CustomR1_PBS2 was used for read 1 (25 cycles) and ORF barcode information was extracted from read 2 (32 cycles), targeting roughly 1×10^3 reads per cell.

FLAG-targeted inCITE-seq library generation

Jurkat KO cells transduced with the lentiviral ORF library (as described above) were harvested from culture and 1×10^6 cells were placed on ice. All subsequent steps (until loading onto the 10x Genomics chip) were performed on ice with prechilled reagents. PBS with FBS and recombinant RNase inhibitor (PBS/FBS/RRI) was prepared as the following mix: 8 ml PBS, 160 ul FBS (2% final), and 80 ul SUPERase-IN RNase Inhibitor (Thermo AM2696, 0.2 U/ul final). Cells were spun down at 350 g for 5 min, resuspended in 100 ul fix buffer (497ul PBS/FBS/RRI, 3.13 ul 16% PFA), and incubated on ice for 10 min. Then 300 ul perm buffer (4.95 ml PBS/FBS/RRI, 50 ul 10% Tween) was added and cells were spun down at 200 g for 5 min. Cells were then gently resuspended in 300 ul perm buffer, incubated on ice for 5 min, and spun down at 200 g. Cells were then gently resuspended in 50 ul block buffer (249 ul perm buffer, 1.25ul HCR probe hybridization buffer from Molecular Instruments). Anti-FLAG Total-seq A antibody (data S2) was added (0.5 ul) and cells were stained for 20 min before two washes in 300 ul perm buffer with 200 g spins and gentle resuspensions. Cells were finally gently resuspended in 150 ul PBS/FBS/RRI, filtered with a 100 um FACS strainer, counted, and loaded on a 10x Chromium Next GEM Chip G with $3{\times}10^4$ cells per channel following the 10x Genomics Chromium Next GEM Single Cell 3′ v3.1 protocol. Generation of ADT and ORF barcode libraries was performed as described above.

Bulk ATAC-seq

The Omni-ATAC protocol was followed largely as published (*77*). In brief, 5×10^4 cells from unstimulated or stimulated LAT KO Jurkat T cells transduced with LAT WT (as described above) were harvested on ice and subjected to nuclei isolation following the Omni-ATAC protocol. Purified ATAC fragments were amplified for eight cycles and purified using SPRIselect beads (1.2x). Libraries were quantified by Qubit and Bioanalyzer before sequencing on an Illumina NextSeq 500 targeting 2×10^7 read-pairs per library. The ENCODE ATAC-seq pipeline (https://github.com/ENCODE-DCC/atac-seq-pipeline) was used for preprocessing, and chromVAR was used to infer transcription factor activities.

Bulk RNA-seq

A modified version of the Smart-seq2 single-cell RNA-seq protocol was used (*78*). Approximately 1×10^6 cells were harvested and total RNA was isolated using the RNeasy Mini Kit (Qiagen 74104). 10 ng of RNA was used as input for the reverse transcription reaction and 12 cycles were performed for the whole transcriptome amplification step. The resulting cDNA (0.375 ng) was used as input to the tagmentation reaction, followed by 12 cycles of indexing PCR. Libraries were purified using SPRIselect beads (0.9x), quantified by Qubit and Bioanalyzer, and sequenced on an Illumina NextSeq 500 targeting 2×10^7 read-pairs per library. The Cumulus Smart-seq2 preprocessing pipeline was used to generate gene expression count matrices which were depth normalized, centered, and scaled across samples for each gene (*79*).

Primary T cell isolation, genetic manipulation, and stimulation for single-cell analysis

Human primary $CD4^+$ T cells were isolated from whole blood acquired from the Massachusetts General Hospital Blood Transfusion Service, following genomic data sharing policy guidelines and in accordance with the Broad Institute Office of Research Subject Protection (ORSP) protocol 3439. Blood donors consented to use their tissue for research purposes. Peripheral blood mononuclear cells (PBMCs) were first isolated from blood using Ficoll-Paque PLUS density gradient media (Cytiva 17144002) following manufacturer's instructions. $CD4^+$ T cells were then isolated using the EasySep Human $CD4^+$ T cell isolation kit (StemCell Technologies 17952). Cells were either cultured directly in RPMI with 10% FBS, Pen/Strep/Glutamine (referred to as RPMI/FBS/PSG, as described above for Jurkat T cells) supplemented with 50 U/ml of IL2 (StemCell Technologies 78036), or cryopreserved in BamBanker Freezing Media (Bulldog Bio BB01). Prior to transduction, $CD4^+$ T cells were expanded with Dynabeads Human T-Activator CD3/CD28 beads (Thermo 11161D) at a 1:1 bead:cell ratio, with approximately 1×10^6 cells in 1ml of media in a 24-well plate.

For transduction of primary T cells, lentivirus was generated in a similar fashion as described above for Jurkat T cells with several modifications. 4.5×10^6 HEK 293T cells were seeded in a 10 cm dish (coated with poly-L-lysine as described above). The following day, cells were transduced with the Lipofectamine 3000 reagent (Thermo Fisher). For each sample, a first mix of 40 ul Lipofectamine 3000 and 1 ml Optimem media was made. A second mix of plasmids (8 ug transfer plasmid, 6 ug psPAX2, and 2 ug pMD2.G (VSV-G) was diluted in 1 ml Optimem, then 32 ul P3000 reagent was added. The plasmid/P3000/Optimem mix was then pipetted on top of the Lipofectamine 3000 plus Optimem mix and incubated for 15 min at RT before the entire resulting volume was gently pipetted onto the cells. The following morning the media was changed. At 48 hours and 72 hours post-transfection, the supernatant was harvested, filtered with a 0.45 um low protein-binding syringe filter (Pall Corporation 4614), mixed with 3 ml Lenti-X concentrator, and incubated at 4C for 1 to 5 days. The resulting mix was spun at 4C at 1500 g for 45 min before supernatant was removed and the combined harvests from 48 hours and 72 hours were resuspended in 200 ul RPMI/FBS/PSG with 50 U/ml IL2. These volumes were divided into 40 ul aliquots and frozen at −80C.

Cells were transduced in a 96-well round-bottom plate, allocating 10 wells for each virus (each encoding one ORF). Cells expanded with Dynabeads (1×10^6 cells in 1 ml media) were first mixed by pipet to separate beads from cells. Then in each well we mixed 35 ul cells (at approximately 1×10^6 cells per ml, not accounting for expected cell expansion), 1 ul Lentiboost (Sirion Biotech SB-P-LV-101-01), 10 ul thawed virus, and 49 ul media with 50 U/ml IL2. This plate was spun for 1 hour at 32C at 931 g and then incubated at 37°C overnight. The following day, 100 ul fresh media was added to each well and wells were pooled for each virus (2 ml total) into a well of a 6-well plate. Dynabeads were then added (4×10^5) to achieve an approximate 2:1 ratio of beads: cells. After two more days of incubation, all cells were pooled, de-beaded using a magnet and counted. The resulting pool was divided into aliquots of 5×10^6 cells for nucleofection.

For nucleofection to knock out endogenous LAT using the Lonza 4D-Nucleofector, we assembled the ribonucleoprotein (RNP) complex using following a protocol similar that used to generate the Jurkat LAT KO cell line. We first annealed 1.65 ul crRNA (200 uM) and 1.65 ul

Downloaded from https://www.science.org at Broad Institute on April 30, 2026

tracrRNA (200 uM) with 4.2 ul IDTE buffer to generate the guide RNA. This mix was heated at 95C for 5 min, then cooled to 75C at 1 C per second, then spun down and left at room temperature (RT) for five minutes. Cas9 V3 product from IDT was diluted in PBS at a ratio of 1.5:1 of Cas9:PBS. The RNP was then assembled by mixing equal volumes of annealed guide RNA with diluted Cas9 protein and incubating at room temperature for 10 to 45 min. IDT enhancer oligo was also diluted in P3 buffer (Lonza) by mixing 2.2ul enhancer oligo (100 uM stock) with 7.8 ul P3 buffer. At this point, 3×10^6 cells per nucleofection sample were spun down in a 1.5ml tube and left at RT. Cells, RNP, fresh RPMI/FBS/PSG, a PCR strip tube, and the 16-well Lonza Nucleocuvette were brought to the nucleofection device. The nucleofector was set to cuvette mode with cell type specified as stimulated primary T cells, program EH-115, and buffer P3. For each sample, 1 ul of diluted enhancer oligo was mixed with 1 ul of RNP in a strip tube. Then one cell pellet sample was gently resuspended in 20 ul P3 buffer and that volume was transferred to the strip tube containing enhancer oligo and RNP. The total resulting volume was mixed gently and transferred to one well of the Nucleocuvette carefully to avoid bubbles. After loading all samples, the Nucleocuvette was tapped to remove bubbles, placed in the nucleofector, the program was run, and the Nucleocuvette was quickly removed. 100 ul RPMI/FBS/PSG (no IL2) was dripped into each well without mixing, and the Nucleocuvette was quickly transferred to a 37C tissue culture incubator for 15 min. Next the cells were transferred to a well of a 12-well plate containing preequilibrated RPMI/FBS/PSG with 500 U/ml IL2. The following morning, cells were spun down and resuspended in 1 ml RPMI/FBS/PSG with 50 U/ml IL2 and incubated overnight. The following day, all cells were pooled, spun down, and resuspended in RPMI/FBS/PSG with 50 U/ml IL2 to a concentration of 1.2×10^6 cells per ml.

After two more days, cells were spun down and resuspended at 1.5×10^6 cells per ml with 0.6 ug/ml puromycin to begin selection. After two more days, cells were counted (viability ~50%). These cells were processed using the EasySep Dead Cell Removal Annexin V Kit (StemCell Technologies), which increased viability to ~70% and cells were maintained at 1.5×10^6 cells per ml with puromycin. At this point a sample of cells was also taken to confirm Cas9 activity by genomic DNA extraction, PCR amplification of the targeted locus, and Sanger sequencing. Using TIDE (*80*) to analyze Sanger sequencing results, we achieved ~75% indel generation.

After two more days, cells were harvested and prepared for TCR stimulation followed by single-cell RNA-seq and ATAC-seq analysis on the 10x Genomics platform, similar to the workflow performed on Jurkat T cells describe above. 2.5×10^5 cells were resuspended in 500ul of media with 50 U/ml IL2 and rested for one to three hours. Then anti-CD3 and anti-IgG antibody were added to wells and mixed to achieve a final 1 ug/ml concentration of each antibody. Cells were incubated for 90 min before harvesting. For scRNA analysis, cells were stained with BioLegend Hashtag B antibodies with barcodes 1 to 4 (following the same protocol for CITE-seq antibody staining described above for Jurkat T cells) to identify each replicate sample. Each replicate sample was counted, mixed evenly, and diluted to 1×10^3 cells per ul before loading 30ul of cells onto two channels of Chip G using the 10x Genomics scRNA v3.1 kit. Gene expression and ORF barcode libraries were generated as described above, and feature barcoding hashtag library was generated following 10x Genomics suggested protocol. For scATAC analysis, cells were processed in a similar fashion as the Jurkat T cell experiment described above. 1.8×10^4 cells from each of two replicate samples were loaded into two channels of Chip H (one sample per channel) using the 10x Genomics scATAC v2 kit. Further processing with Spear-ATAC modifications for ORF barcode recovery was performed as described above for the Jurkat T cell experiment.

LAT protein proximity labeling with TurboID in activated T cells

The lentiviral expression vector described above was modified to express LAT with a C-terminal TurboID fusion. In brief, we designed an IDT gBlock Gene Fragment encoding a glycine-serine linker, TurboID (sequence derived from Addgene plasmid 107169), and a V5 tag (data S2). A PCR amplicon encoding LAT with overhangs for cloning was generated using primers Fwd_LAT_forTurboID and Rev_LAT_forTurboID. The amplicon was agarose gel purified, and the product was used for an In-Fusion (Takara Bio 638947) cloning reaction with the following components: 1ul In-Fusion master mix, 1ul of p_sc_eVIP vector (digested with NheI for 2 hours and gel purified) at 100 ng/ul, 0.5 ul LAT PCR amplicon at 70 ng/ul, 0.5 ul TurboID gBlock at 50 ng/ul, and 2 ul water. After a 15 min incubation at 50C, 2.5ul of this reaction was used to transform approximately 20 ul of NEB Stable Competent *E. coli* (New England Biolabs C3040H). Bacteria were grown at 30C to prevent recombination of lentiviral repeat regions. A single colony was picked from an LB agar plus ampicillin plate and grown overnight in LB media with ampicillin for miniprep and Sanger sequencing validation.

To detect LAT proximal proteins by Western blot we followed an established protocol (*81*) with some modifications. Lentivirus was generated using the LAT-TurboID transfer vector as described above, and LAT KO Jurkat T cells were transduced and selected as described above. For each stimulation and labeling experiment, 1.5×10^6 transduced cells were rested for 1 hour in 1 ml in a 12-well plate in a 37C incubator. We used the phosphatase inhibitor pervanadate to stimulate cells, an approach which mimics direct TCR stimulation but yields a stronger, more durable response to facilitate protein interaction detection (*82*–*84*). 100x concentrated pervanadate was made as a mix of 300 mM hydrogen peroxide (from a fresh bottle within ten days of opening) and 10 mM sodium orthovanadate in water. We then added 10 ul of 100x pervanadate to 1 ml of cells, mixed the samples, and returned the plate to the incubator for ten minutes of labeling. No exogenous biotin was added to the culture (the level of biotin in RPMI 1640 media was sufficient for robust labeling). The plate was then placed on ice, and cells were transferred to 1.5 ml tubes for three washes in 1 ml of DPBS at 4C at 400 g. For each wash, we took care to remove all supernatant by first removing 900 ul of supernatant for all samples and then removing the remaining ~100 ul in a quick aspiration step.

Cells were then lysed by resuspending in 100 ul RIPA buffer with 1x protease inhibitor cocktail (Millipore Sigma P8849) and 1 mM PMSF (VWR 82021-256), thoroughly pipet mixing, and incubating on ice for 10 min. Samples were then spun at 4C at 13×10^3 g for 10 min to clarify the lysate. 5 ul of clarified lysate was taken as an input sample and mixed with 5 ul reducing Laemmli buffer (Boston Bioproducts BP-111R) and 20 ul water, then boiled for 5 min at 95C. 90 ul of clarified lysate was mixed with Pierce Streptavidin Magnetic Beads (Thermo Fisher 8816) resuspended in 500 ul RIPA buffer (25ul beads stock per sample) in a 1.5 ml tube. Streptavidin pull-down of biotinylated proteins was performed for 2 to 3 hours by rotating samples at 4C. Bead washing was performed using a magnetic rack in an ice bucket with buffers prechilled and 900 ul buffer per wash. For each wash, tubes were quickly transferred from one side of the magnet rack to the other and then returned to the original side to ensure bead mixing. The following washes were performed: two washes with RIPA (two transfers each), one wash with 1M KCl (two transfers), one wash with 0.1M Na2CO3 (one transfer), one wash with 2M urea (in 10 mM Tris-HCl pH 8) (one transfer), and two washes in RIPA (two transfers each). After removal of the last wash buffer, tubes were quickly spun down with a bench-top centrifuge and returned to the magnet to remove all supernatant. Then 40 ul elution buffer (150ul 6x Laemmli buffer, 6 ul 0.1M biotin, 144 ul water) was added to each well and samples were spun again quickly. A p20 pipet was then used to thoroughly resuspend the beads in elution buffer, with vigorous pipetting approximately ten times. Samples were then boiled for 10 min at 95C to elute proteins. Tubes were spun again quickly and returned to the magnet, and after 30 s the elution volume was transferred to a fresh tube.

Downloaded from https://www.science.org at Broad Institute on April 30, 2026

We then ran a Western blot using the NuPAGE Bis-Tris gel system (Thermo Fisher) with 5 ul input and 15 ul enrichment for each sample along with 4 ul Precision Plus Protein standard (Bio-Rad 1610374). The gel was separated at 180 V for 30 min, followed by a transfer using the iBlot2 system nitrocellulose membranes with the P0 protocol. The membrane was cut horizontally at preidentified sizes for PLCG1 (Cell Signaling 2822S, RRID:AB_2163702), GAPDH (Thermo Fisher PA1-987, RRID:AB_2107311), and GRB2 (Thermo Fisher PA5-27151, RRID:AB_2544627), and incubated overnight with 1:1000 primary antibody in TBS-T with 5% milk at 4C on a rocking mixer. The following day, membranes were washed three times in TBS-T for 5 min each and incubated in 1:2000 secondary antibody targeting Rabbit IgG conjugated to HRP (Thermo Fisher A27036, RRID:AB_2536099) in TBS-T with 5% milk at RT on a rocking mixer. Membranes were again washed three times in TBS-T for 5 min each, and ECL reagent (Sigma GERPN2232) was used to visualize proteins on a Bio-Rad ChemiDoc MP imager. Bands were quantified using the FIJI Analyze Gels function. Normalized enrichment values were calculated by dividing the enrichment band value by the mean of the input value for GAPDH and PLCG1. Means and error bars in Fig. 4 represent values from four replicate experiments performed on four separate days.

Jurkat T cell TCR stimulation and flow cytometry to detect surface proteins

LAT KO Jurkat T cells were transduced with lentivirus expressing a single ORF and selected with puromycin as described above. 2×10^5 cells per ORF were deposited in two replicate wells for an unstimulated condition and two replicate wells for a stimulated condition in 200 ul media in a 96-well flat-bottom plate. Cells were equilibrated for three hours before addition of anti-CD3 antibody for a final concentration of 0.1 ug/ml and mixed with a multi-channel pipet. After six hours, cells were transferred to a v-bottom 96-well plate, spun at 350 g for 5 min at 4C in a swinging-bucket centrifuge, and resuspended in 50 ul PBS plus 2% FBS containing 1:100 diluted anti-CD69-APC antibody (BioLegend 310909, RRID:AB_314844). Cells were stained in the dark on ice for 30 min, then 200 ul PBS + 2% FBS was added and cells were washed twice in the same buffer before a final resuspension in 200 ul of the same buffer. Cells were analyzed on a Beckman CytoFLEX flow cytometer. Mean APC values were calculated for each sample and normalized to value for cells expressing WT LAT.

Jurkat T cell stimulation, nuclei isolation, and flow cytometry to detect nuclear transcription factors

Cells were analyzed by nuclear antibody staining and flow cytometry using a method adapted from the laboratory of Leslie Berg (Gallagher *et al*., *PNAS*, 2021) (*33*). LAT KO Jurkat T cells were transduced with lentivirus expressing a single ORF and selected with puromycin as described above. 4×10^5 cells per ORF were then deposited into wells of a 96-well U-bottom plate and equilibrated for one to three hours before addition of anti-CD3 and anti-IgG antibodies for a final concentration of 1 ug/ml of each antibody. Cells were mixed with a multi-channel pipet and returned to the incubator for one hour. The plate was then placed on ice and then spun at 350 g for 5 min at 4C in a swinging-bucket centrifuge. Nuclei isolation was then performed in the plate, following the 10x Genomics ATAC nuclei isolation protocol with slight adjustments and using multi-channel pipettes. Cells were washed with PBS containing 0.01% BSA, then resuspended with ten aspiration/dispense steps in 100 ul of ATAC lysis buffer with the addition of protease inhibitor cocktail (1:100 dilution of Millipore Sigma P8849) and PMSF at 1 mM (VWR 82021-256). Cells were incubated on ice for 3 min, and then 200 ul of 10x ATAC wash buffer (with the addition of protease inhibitor cocktail and PMSF) was added, cells were mixed, and the plate was spun at 500 g for 5 min at 4C. Pelleted nuclei were then resuspended in 100 ul of fixation buffer from the eBioscience Foxp3 / Transcription Factor Staining Buffer Set (Thermo Fisher 00-5523-00). Nuclei were fixed for 30 min on ice before addition of 200 ul of permeabilization buffer (from the Foxp3 kit) and spun again (all subsequent spins were 500 g for 5 min at 4C). Nuclei were resuspended in 200 ul permeabilization buffer, split evenly into replicate wells for separate staining of each antibody, and spun again. Nuclei were then resuspended in 50 ul of permeabilization buffer containing 100x dilution of either anti-cFos (Cell Signaling 2250S, RRID:AB_2247211) or anti-NFATC1 (Cell Signaling 5861S, RRID:AB_10834808) antibodies. This primary antibody incubation was performed for 30 min before addition of 200 ul of permeabilization buffer, pelleting, resuspension in permeabilization buffer, pelleting, and resuspension in 50ul of permeabilization buffer containing 1000x dilution of anti-Rb IgG AF647 secondary antibody (BioLegend 406414). Nuclei were incubated in the dark for 20-40 min before addition of 200ul permeabilization buffer, pelleting, and two subsequent washes with permeabilization buffer. Finally, nuclei were resuspended in 200ul of PBS containing 2% FBS and 8 mM MgCl2. Nuclei were analyzed on a Beckman CytoFLEX flow cytometer.

Jurkat T cell stimulation, whole cell fixation, and flow cytometry to detect phospho-ERK

LAT KO Jurkat T cells were transduced with lentivirus expressing a single ORF and selected with puromycin as described above. $4{\times}10^5$ cells per ORF were then deposited into wells of a 96-well U-bottom plate and equilibrated for one to three hours before addition of anti-CD3 and anti-IgG antibodies for a final concentration of 1 ug/ml of each antibody. Cells were mixed with a multi-channel pipet and returned to the incubator for 15 min. The plate was then placed on ice and spun at 350 g for 5 min at 4C in a swinging-bucket centrifuge. Cells were resuspended in 50 ul of 4% PFA in PBS, gently mixed ten times, and incubated for 10 min on ice. We then added 200 ul PBS, spun the plate, and resuspended cells gently in 25 ul PBS. We then added 200 ul of ice-cold methanol, gently mixed, and incubated on ice for ten minutes. The plate was then spun, cells were resuspended in 200 ul PBS + 2% FBS to wash, and the plate was spun again. Cells were then resuspended in 50 ul PBS + 2% FBS containing a 1:100 dilution of anti-phospho-Erk (Thr202/Tyr2040) (Cell Signaling 9101S), and incubated on ice for 30 min. We then added 200 ul PBS + 2% FBS, spun the plate, resuspended in 200ul PBS + 2% FBS to wash, and spun the plate again before resuspending in 50ul PBS + 2% FBS containing a 1:1000 dilution of anti-Rb IgG AF647 secondary antibody (BioLegend 406414, RRID:AB_2563202). Cells were incubated on ice in the dark for 20-40 min before addition of 200 ul PBS + 2% FBS, pelleting, and two subsequent washes with PBS + 2% FBS before a final resuspension in 200 ul PBS + 2% FBS.

TCR delivery to Jurkat T cells and stimulation via coculture with peptide-MHC–expressing K562 cells

A lentiviral plasmid expressing the 1G4 TCR beta chain – T2A – 1G4 TCR alpha chain - IRES – EGFR fragment was received from the laboratory of Michael Birnbaum at MIT, and is similar to previously described plasmids (Dobson *et al*., *Nature Methods*, 2022) (*85*). The 1G4 TCR was derived from a human melanoma patient and has been characterized to bind a peptide derived from the tumor antigen NY-ESO-1 and presented on HLA-A2 (Robbins *et al*., *Journal of Clinical Oncology*, 2011) (*54*).

We first generated LAT KO Jurkat T cells stably expressing the 1G4 TCR by transducing LAT KO T cells with lentivirus encoding 1G4-IRES-EGFR. Transduced cells were sorted for high levels of the EGFR marker after staining with PE-conjugated anti-EGFR antibody (BioLegend 352903, RRID:AB_10898161). The resulting 1G4 LAT KO Jurkat T cells were then transduced with lentivirus expressing a single LAT variant or GFP control ORF and selected with puromycin as described above.

A lentiviral plasmid encoding the single-chain-trimer of 9V peptide derived from NY-ESO-1 antigen beta-2-microglobulin, and HLA-A2 as well as mCherry was derived from a previously described plasmid

Downloaded from https://www.science.org at Broad Institute on April 30, 2026

received from the laboratory of David Baltimore at the California Institute of Technology (Li, Bethune *et al*., *Nature Methods,* 2019) (*55*). K562 cells were transduced with lentivirus generated from this plasmid and sorted for high expression of mCherry.

To stimulate T cell activation we generally followed a protocol described for the activation of mouse T cells with antigen presenting cells (Gallagher *et al*., *PNAS,* 2021). 2×10^5 LAT KO Jurkat T cells expressing 1G4 TCR and a LAT variant or GFP ORF were first seeded into a 96-well U-bottom plate in 100 ul of normal growth media. Separately, K562 cells expressing NY-ESO-1 pMHC were washed twice in PBS and labeled using CellTrace Yellow (Thermo Fisher C34567) for 20 min before a wash in normal growth media. In a separate well, 4×10^5 labeled K562 cells expressing NY-ESO-1 pMHC were seeded in 100 ul media and the plate was equilibrated for one to three hours. Jurkat cells were then deposited into wells containing K562 cells, the whole well was mixed five times gently, and the plate was spun for 30 s at 300 g to create a loose cell pellet before returning to the incubator for indicated amounts of time. Cells were then processed for nuclei isolation and staining as described above for cells stimulated with antibodies, with the exception that an additional flow cytometry gate to separate CellTrace Yellow-positive K562 nuclei from CellTrace Yellow-negative Jurkat nuclei was added.

Jurkat T cell stimulation via coculture with peptide-pulsed T2 antigen presenting cells

LAT KO Jurkat T cells stably expressing the 1G4 TCR and single LAT variants or GFP were generated as in the section above describing the experiment stimulating Jurkat cells with peptide-MHC-expressing K562 cells. To stimulate T cell activation we generally followed the protocol described above for stimulation with peptide-MHC-expressing K562 cells. T2 antigen presenting cells (ATCC CRL-1992) were grown in the same culture conditions as Jurkat T cells. NY-ESO-1-derived peptides were purchased from GenScript (TurboTide product), resuspended in DMSO to 5 mg/ml and stored in aliquots at -20C. Peptide sequences were as follows, with affinities derived from a previous study (*86*): NY-ESO-1 3Y (sequence SLYMWITQC, affinity 36.3 uM); NY-ESO-1 6T (sequence SLLMWTTQC, affinity 84.6 uM); NY-ESO-1 5Y (sequence SLLMYITQC, affinity 191 uM).

1×10^5 LAT KO Jurkat T cells expressing 1G4 TCR and a LAT variant or GFP ORF were first seeded into a 96-well U-bottom plate in 100 ul of normal growth media. Separately, 4×10^6 T2 cells were washed twice in PBS and labeled using 1 ul CellTrace Yellow (Thermo Fisher C34567) in 1 ml PBS for 20 minutes before a wash in normal growth media. Labeled T2 cells were resuspended in 1 ml of growth media to achieve a concentration of 2×10^6 cells/ml. For each peptide analyzed, 220 ul of labeled T2 cells was mixed with 220 ul peptide diluted to 0.4 ug/ml in media. 100 ul of this T2 cell with peptide mix was then deposited into wells of the 96-well U bottom plate, and the plate was placed in the cell culture incubator for one hour to allow for cell equilibration and peptide loading. The cell suspensions of Jurkat cell wells were then transferred into wells containing labeled, peptide-pulsed T2 cells, the whole well was mixed five times gently, and the plate was spun for 30 seconds at 300g to create a loose cell pellet before returning to the incubator for one hour to allow for stimulation. Cells were then processed for nuclei isolation and staining as described above for cells stimulated with antibodies, with the exception that an additional flow cytometry gate to separate CellTrace Yellow-positive T2 nuclei from CellTrace Yellow-negative Jurkat nuclei was added.

Coimmunoprecipitation to detect GRB2-interacting proteins in activated T cells

Lentivirus was generated using the LAT transfer vector and LAT KO Jurkat T cells were transduced and selected as described above. Prior to harvesting cells, Invitrogen Dynabeads Protein G (Thermo Fisher 10003D) were bound with anti-GRB2 antibody (Thermo Fisher PA5-27151, RRID:AB_2544627). For binding, we thoroughly resuspended the beads, transferred 25 ul of beads per sample to a 1.5 ml tube, placed the tube on a magnetic rack, removed the supernatant, and resuspended the beads in 100 ul of PBS plus 0.01% Tween-20 per sample. Resuspended beads were then mixed with 1 ul (corresponding to 1 ug) of anti-GRB2 antibody per sample, mixed, and incubated on a rotator at RT for 10 min. Following incubation, the tube was returned to the magnetic rack, supernatant was removed, and beads were resuspended in 100 ul of PBS plus 0.01% Tween-20 per sample and left at RT until after the preparation of the clarified cell lysate.

For each stimulation and immunoprecipitation (IP) experiment, 1×10^7 transduced cells were harvested in a 1.5 ml tube, resuspended in 100 ul PBS, and equilibrated to 37C in a heat block for five minutes. We used the phosphatase inhibitor pervanadate to stimulate cells as detailed above in the methods section describing the TurboID labeling experiment. We diluted 100x pervanadate (freshly prepared immediately before use) further to 2x using PBS, added 100 ul 2x pervanadate to each sample of cells, and incubated cells for five minutes in a heat block. Tubes were then placed on ice and cells were lysed by the addition of 200 ul of cold 2x Brij lysis buffer (Brij 97 [Millipore Sigma P6136] 2%, Tris-HCl 50 mM, NaCl 300 mM, EDTA 10 mM) containing PhosSTOP (Millipore Sigma 4906845001) as well as 1% protease inhibitor cocktail (Millipore Sigma P8849) and 1 mM PMSF (Millipore Sigma 10837091001). Samples were mixed gently by pipet and incubated on ice for 10 min. Samples were then spun at 4C at 13×10^3 g for 10 min to clarify the lysate. 15 ul of clarified lysate was taken as an input sample and mixed with 5 ul reducing Laemmli buffer (Boston Bioproducts BP-111R) and 10 ul water, then boiled for 10 min at 95C.

Antibody-loaded beads were placed on the magnetic rack and resuspended in 50 ul of 1x Brij buffer containing PhosSTOP (not including protease inhibitor cocktail or PMSF) per sample. 50 ul of resuspended antibody-bound beads were then transferred to a fresh 1.5 ml tube for IP. For each sample, 350 ul of clarified lysate was added to the corresponding tube of antibody-bound beads on ice and gently mixed. IP was performed for 90 min at 4C with rotation in a cold room.

One round of bead washing was then performed using a prechilled magnetic rack in the cold room with 500 ul of wash buffer composed of 1x Brij buffer containing PhosSTOP (not including protease inhibitor cocktail or PMSF). For the wash, tubes were placed on the magnetic rack, supernatant was removed, wash buffer was added, and each tube transferred from one side of the magnetic rack to the other and then returned to the original side. This transfer (without removal or addition of wash buffer) was repeated once. After removal of the wash buffer, tubes were quickly spun down in a bench-top centrifuge and returned to the magnet to remove all supernatant. Then 40 ul elution buffer (150 ul 6x Laemmli-reducing buffer, 150 ul water) was added to each tube and samples were spun in a bench-top centrifuge again quickly to collect beads in the elution buffer. A p20 pipet was then used to thoroughly resuspend the beads in elution buffer, with vigorous pipetting and scraping the bottom of the tube with the pipet tip approximately ten times. Samples were transferred to a strip tube and boiled for 10 min at 95C. Tubes were spun again quickly, placed on a strip tube magnet, and after 30 s the elution volume was transferred to a fresh strip tube.

We then ran a Western blot using the NuPAGE Bis-Tris gel system (Thermo Fisher) with 5 ul input and 15 ul enrichment for each sample along with 4 ul Precision Plus Protein standard (Bio-Rad 1610374). The gel was separated at 180 V for 30 min, followed by a transfer using the iBlot2 system nitrocellulose membranes with the P0 protocol. The membrane was cut horizontally at preidentified sizes for PLCG1 (Cell Signaling 2822S, RRID:AB_2163702) and GAPDH (Thermo Fisher PA1-987, RRID:AB_2107311), and incubated overnight with 1:1000 primary antibody (PLCG1) or 1:2000 primary antibody (GAPDH) in TBS-T with 5% milk at 4C on a rocking mixer. The following day, membranes were washed three times in TBS-T for 4 min each and incubated in 1:2000 secondary antibody targeting Rabbit IgG conjugated to HRP (Thermo Fisher A27036) in TBS-T with 5% milk at RT for 30 min on a rocking mixer. Membranes were again washed three times in TBS-T for 4 min

Downloaded from https://www.science.org at Broad Institute on April 30, 2026

each, and ECL reagent (Sigma GERPN2232) was used to visualize proteins on a Bio-Rad ChemiDoc MP imager. Bands were quantified using the FIJI Analyze Gels function. Normalized enrichment values were calculated by dividing the enrichment band value by input value for GAPDH. Means and error bars in fig. S13, C and D represent values from three replicate experiments performed on three separate days.

Imaging of PLCG1 and GRB2 in primary mouse T cells

Detailed methods can be found in our previous work (*61*, *87*–*89*). In brief, murine T cells were harvested from lymph nodes and spleens from 8-week-old mice. Animals were the cross of (B10.Cg- Tg(TcrAND)53Hed/J) x(B10.BR-H2k2 H2-T18a/SgSnj) from Jackson Laboratory. IL-2 treated T cell blasts were transduced using retroviruses produced in Platinum-E Retroviral Packaging Cell Line (Cell Biolabs, Inc. RV-101) derived supernatants. The retroviral vector, MSCV-PLCG1$_{SHarray}$ -mNG-P2A-mSC-Grb2, was used for transduction. PLCG1$_{SHarray}$ consists of the truncated nSH2, cSH2, and SH3 domains of PLCG1 that are involved in interaction with LAT and SLP76. This fragment was cloned from mouse PLCG1 cDNA obtained from Horizon Discovery. The GRB2 sequence was obtained from a plasmid containing human GRB2 that was a gift from Neel Shah (*90*). Plasmid and licenses for mNeonGreen (mNG) and an mScarlet (mSC) were purchased from Allele Biotechnology. Supported lipid bilayer membranes were prepared in imaging chambers and then functionalized with mouse ICAM-1 and peptide-loaded MHC (pMHC), as described in our previous work. Here, pMHC was prepared by incubating MCC (ANERADLIAYLKQATK)-GGSC-Atto647N with MHC II I-E^{k} at 37°C in peptide loading buffer. Supported bilayers were prepared on etched cover glasses using small unilamellar vesicles containing the following components: 98 mol% 1,2-dioleoyl-sn-glycero-3-phosphocholine (DOPC, Avanti Polar Lipids) and 2 mol% 1,2-dioleoyl-sn-glycero-3-[(N-(5-amino-1-carboxypentyl)iminodiacetic acid)succinyl] nickel salt (DGS-NTA, Avanti Polar Lipids). ICAM-1 (1.3 nM, estimated density ~100 μm^{-2}) and pMHC (concentration adjusted, 1-6 pM for 0.1-0.6 μm^{-2}) were then added to the chambers for functionalization. All imaging experiments were performed on a motorized inverted microscope (Nikon Eclipse Ti-E; Technical Instruments, Burlingame, CA) with a motorized Epi/TIRF illuminator, and a motorized stage (MS-2000; Applied Scientific Instrumentation, Eugene, OR). Details of microscope setup can be found in our previous work. Imaging analysis was conducted using the standard TrackMate plugin (*91*) for ImageJ in conjunction with a custom Python code script to generate image tiles in fig. S14B. PLCG1$_{SHarray}$ localization spots (0.5 μm diameter in size) were initially tracked via TrackMate's automated workflows, and then each track was manually refined for accurate linking and detection. GRB2 localization was scored positive if GRB2 intensity at the PLCG1$_{SHarray}$ spot shared a kinetic growth profile and if the GRB2 signal vs. background exceeded by a factor of approximately 1.5 or more.

Single-cell RNA-seq and ATAC-seq data preprocessing and ORF barcode assignment

For gene expression, ADT, HTO, and scATAC libraries, Cellranger preprocessing with standard parameters from the Cumulus V2.1.1 instance was used to generate cell-level expression matrices as well as chromatin accessibility peaks and fragment files (*79*). Seurat v4.3.0 was used to process scRNA, ADT, and HTO libraries (*92*). Cells were filtered for number of genes (between 5×10^2 and 1×10^4) and mitochondrial content (up to 10%). Gene expression matrices were then normalized using SCTransform in Seurat using parameters vst.flavor = "v2." SCT residuals were used for all further analyses. Signac v1.9.0 was used with Ensembl database EnsDb.Hsapiens.v86 and hg38 to process scATAC data (*93*). Cells were filtered for peak region fragments (1×10^3 to 3×10^4), percent reads in peaks (>15%), nucleosome signal (<4), and transcription start site enrichment (>2). ChromVAR was run within Signac using the JASPAR 2020 motif database and deviation values were used as inferred TF (motif) activities for all further analyses.

Custom UNIX and Python scripts were used to process fastq files from ORF barcode libraries into per-cell counts of ORF barcodes from a register of the library barcodes and are available to download from Zenodo (*94*). ORF barcode counts were normalized by total counts per cell, and cells were thresholded on a minimum total counts for CITE-seq (50 reads) and proportion of reads supporting the top ORF barcode (80% for Spear-ATAC and CITE-seq) based on analysis of the distribution of proportions. The top ORF barcode in each cell was assigned as the ORF identity.

Generation and statistical analysis of ORF-level activation scores and feature values

A single-cell sampling approach was implemented to understand the probability of observing by chance a given effect size in a set of cells of a certain size. First, an activation score for each cell was calculated for each time point. To generate a chromatin score from ATAC data, the top 50 TF motifs with greater chromVAR signal in cells expressing WT LAT versus cells expressing GFP were averaged. For RNA samples, the top 50 genes with greater SCT residuals in cells expressing WT LAT versus cells expressing GFP were averaged. To determine statistical significance of scores for cells associated with a particular ORF deviating from WT LAT, the scores for each cell expressing an ORF were averaged and 1,000 samples, each matched to the number of cells supporting the ORF being examined, were taken from each of the three WT LAT replicate cell pools. For each sample, the average score across cells was calculated and the difference in score between sampled cells and the WT replicate pool from which it was sampled was determined. For each WT replicate sample, the number of instances in which the sample had a more extreme value than the value observed for the cells expressing the ORF was counted, and the highest proportion (among the three WT replicates) was recorded as the empirical *P* value. The same approach was used to determine *P* values for individual feature values (TF motifs, genes, or CD69 protein). This sampling strategy is modeled in fig. S3C.

To determine ORF clusters, a matrix of chromatin and RNA scores from each time point was clustered using the R k.means function with default parameters and k=3.

Annotation of LAT protein sequence features with the Eukaryotic Linear Motif Database and localCIDER

The amino acid sequence of LAT (ENST00000395456) was entered into the Eukaryotic Linear Motif resource website (www.elm.eu.org) using all cell compartments and a default motif probability cutoff of 100. The resulting table was downloaded and processed in R to display the visualization in Fig. 2. LAT homolog protein sequences were extracted from the ConSurf tool output (https://consurf.tau.ac.il/consurf_index.php). To determine amino acid sequence identity of each homolog compared to human LAT, NCBI BLASTP was performed using default parameters. A random set of 100 human length-matched proteins was derived from the UniProt database website after filtering for homo sapiens (organism ID 9606) and "Reviewed" proteins. The resulting fasta file was processed in Python to extract 100 random proteins with length between 200 and 250 amino acids to approximate the length of LAT. To calculate biophysical sequence features, localCIDER was run using Python to analyze all LAT ortholog sequences and random background proteins.

Prediction of protein binding to LAT with AlphaFold-Multimer

AlphaFold-Multimer was run using Colabfold V1.5.5 via Docker (https://ghcr.io/sokrypton/colabfold:1.5.5-cuda11.8.0) on a Google cloud project virtual machine (NVIDIA T4 GPU with 30GB memory) (*95*). We generally followed instructions described on the associated GitHub (https://github.com/sokrypton/ColabFold/wiki/Running-ColabFold-in-Docker). Predictions were generated without templates or relaxation, and MMseqs2 server was used for multiple sequence alignments (paired and

Downloaded from https://www.science.org at Broad Institute on April 30, 2026

unpaired). Sequences for full length proteins and SH2 domains were retrieved from Uniprot. To further interpret the output of Colabfold, we implemented a recently described workflow in Python which parses the structure files [protein data bank) (PDB) format] and AlphaFold-Multimer confidence metrics to identify confident contact regions between two protein chains (*96*, *97*). To generate ten unique models (instead of the maximum of five) when analyzing isolated SH2 domains interacting with LAT, we ran Colabfold a second time with a different random seed. The 10 PDB files representing 10 output models from each SH2 domain were then analyzed using a custom Python script in Pymol to determine the distance between each LAT tyrosine and residue 48 in the SH2 domain, which consistently represented the proximal residue to the LAT tyrosine in interacting structures. A structure was scored as an interaction if the SH2 domain distance to the most proximal tyrosine was less than 10 angstroms and the second nearest tyrosine was at a distance greater than ten angstroms.

Determination of coordinated and biased signaling outputs from chromatin accessibility data

To determine whether individual ORFs conferred coordinated (loss of both AP-1 and NFAT) or biased (loss of either AP-1 or NFAT) inferred TF activity, we identified genomic regions that represent the exclusive (nonoverlapping) activity of each TF on dynamic accessibility in T cell activation. To identify dynamic, stimulation-dependent accessible regions, we counted the total ATAC read counts in cells expressing WT LAT or, separately, in the GFP control in all genomic regions detected at each time point. The resulting matrix (rows = genomic regions, columns = WT LAT or GFP) was depth normalized to $1{\times}10^6$ counts per ORF (WT LAT or GFP), quantile normalized, and scaled using log2(n+1) transformation. Then for each region, the normalized and scaled values for GFP were subtracted from WT to determine the fold change (in log2 units). Regions exhibiting at least 0.5 unit greater signal in WT LAT vs. GFP and at least 1.5 unit average signal (across WT LAT and GFP) were considered stimulation-dependent. Within this set of regions, we identified sites that matched the FOS motif (excluding any sites also matching the NFATC1 motif), or sites that matched the NFATC1 motif (excluding any sites also matching the FOS motif), using motif match information from the AddMotifs function in Signac based on the JASPAR2020 position frequency matrices.

For each ORF, we then calculated the average accessibility in either TF-associated set of regions across all cells expressing the associated ORF to generate a filtered-region TF activation score. These scores were scaled similarly to the chromatin activation score, such that 0 represented the mean value of GFP-expressing cells and 1 represented the mean value of WT LAT-expressing cells. These values were then averaged across the 30 and 90 min. stimulation experiments, and only ORFs supported by more than 40 cells in each time point were analyzed. An ORF was considered to confer a significant defect for a TF activity if the permutation-based *P* value (described above) met a threshold of 0.05 in both time points. ORFs were classified as coordinated if AP-1 (FOS motif) and NFAT (NFATC1 motif) were significantly defective. An ORF was classified as biased if either AP-1 or NFAT were significantly defective in both time points and the other TF had a confidently unaltered response with a *P* value threshold of 0.1 in both time points.

For the analysis of the expanded set of seven motifs in fig. S10, a similar filtering based on stimulation-dependent accessibility was performed and motif overlap filtering was performed such that regions associated with a particular motif did not contain motif matches for any of the other six motifs.

REFERENCES AND NOTES

1. F. Macián *et al.*, Transcriptional mechanisms underlying lymphocyte tolerance. *Cell* **109**, 719–731 (2002). doi: 10.1016/S0092-8674(02)00767-5; pmid: 12086671
2. L. Balagopalan, N. P. Coussens, E. Sherman, L. E. Samelson, C. L. Sommers, The LAT story: A tale of cooperativity, coordination, and choreography. *Cold Spring Harb. Perspect. Biol.* **2**, a005512 (2010). doi: 10.1101/cshperspect.a005512; pmid: 20610546
3. B. Malissen, C. Grégoire, M. Malissen, R. Roncagalli, Integrative biology of T cell activation. *Nat. Immunol.* **15**, 790–797 (2014). doi: 10.1038/ni.2959; pmid: 25137453
4. W. Zhang *et al.*, Association of Grb2, Gads, and phospholipase C-γ 1 with phosphorylated LAT tyrosine residues. Effect of LAT tyrosine mutations on T cell antigen receptor-mediated signaling. *J. Biol. Chem.* **275**, 23355–23361 (2000). doi: 10.1074/jbc.M000404200; pmid: 10811803
5. J. Lin, A. Weiss, Identification of the minimal tyrosine residues required for linker for activation of T cell function. *J. Biol. Chem.* **276**, 29588–29595 (2001). doi: 10.1074/jbc.M102221200; pmid: 11395491
6. W. Zhang, J. Sloan-Lancaster, J. Kitchen, R. P. Trible, L. E. Samelson, LAT: The ZAP-70 tyrosine kinase substrate that links T cell receptor to cellular activation. *Cell* **92**, 83–92 (1998). doi: 10.1016/S0092-8674(00)80901-0; pmid: 9489702
7. T. S. Finco, T. Kadlecek, W. Zhang, L. E. Samelson, A. Weiss, LAT is required for TCR-mediated activation of PLCgamma1 and the Ras pathway. *Immunity* **9**, 617–626 (1998). doi: 10.1016/S1074-7613(00)80659-7; pmid: 9846483
8. W. L. Lo *et al.*, Lck promotes Zap70-dependent LAT phosphorylation by bridging Zap70 to LAT. *Nat. Immunol.* **19**, 733–741 (2018). doi: 10.1038/s41590-018-0131-1; pmid: 29915297
9. M. Martínez-Florensa *et al.*, Serine residues in the LAT adaptor are essential for TCR-dependent signal transduction. *J. Leukoc. Biol.* **89**, 63–73 (2011). doi: 10.1189/jlb.0509342; pmid: 20940326
10. V. N. Uversky, Intrinsically disordered proteins and their "Mysterious" (meta)physics. *Front. Phys.* **7**, fphy.2019.00010 (2019). doi: 10.3389/fphy.2019.00010
11. P. E. Wright, H. J. Dyson, Intrinsically disordered proteins in cellular signalling and regulation. *Nat. Rev. Mol. Cell Biol.* **16**, 18–29 (2015). doi: 10.1038/nrm3920; pmid: 25531225
12. M. Kumar *et al.*, ELM-the eukaryotic linear motif resource in 2020. *Nucleic Acids Res.* **48**, D296–D306 (2020). doi: 10.1038/nrm3920; pmid: 31680160
13. H. R. Kilgore *et al.*, Protein codes promote selective subcellular compartmentalization. *Science* **387**, 1095–1101 (2025). doi: 10.1126/science.adq2634; pmid: 39913643
14. T. Zarin *et al.*, Identifying molecular features that are associated with biological function of intrinsically disordered protein regions. *eLife* **10**, 1–36 (2021). doi: 10.7554/eLife.60220; pmid: 33616531
15. A. L. Sanborn *et al.*, Simple biochemical features underlie transcriptional activation domain diversity and dynamic, fuzzy binding to Mediator. *eLife* **10**, e68068 (2021). doi: 10.7554/eLife.68068; pmid: 33904398
16. J. H. Lobel, N. T. Ingolia, Deciphering disordered regions controlling mRNA decay in high-throughput. *Nature* **642**, 805–813 (2025). doi: 10.1038/s41586-025-08919-x; pmid: 40269159
17. D. M. Fowler, S. Fields, Deep mutational scanning: A new style of protein science. *Nat. Methods* **11**, 801–807 (2014). doi: 10.1038/nmeth.3027; pmid: 25075907
18. G. M. Findlay *et al.*, Accurate classification of BRCA1 variants with saturation genome editing. *Nature* **562**, 217–222 (2018). doi: 10.1038/s41586-018-0461-z; pmid: 30209399
19. A. O. Giacomelli *et al.*, Mutational processes shape the landscape of TP53 mutations in human cancer. *Nat. Genet.* **50**, 1381–1387 (2018). doi: 10.1038/s41588-018-0204-y; pmid: 30224644
20. S. Boettcher *et al.*, A dominant-negative effect drives selection of *TP53* missense mutations in myeloid malignancies. *Science* **365**, 599–604 (2019). doi: 10.1126/science.aax3649; pmid: 31395785
21. M. V. Staller *et al.*, Directed mutational scanning reveals a balance between acidic and hydrophobic residues in strong human activation domains. *Cell Syst.* **13**, 334–345.e5 (2022). doi: 10.1016/j.cels.2022.01.002; pmid: 35120642
22. R. Kagawa *et al.*, Alanine-scanning mutagenesis of human signal transducer and activator of transcription 1 to estimate loss- or gain-of-function variants. *J. Allergy Clin. Immunol.* **140**, 232–241 (2017). doi: 10.1016/j.jaci.2016.09.035; pmid: 28011069
23. S. Brodsky *et al.*, Intrinsically Disordered Regions Direct Transcription Factor In Vivo Binding Specificity. *Mol. Cell* **79**, 459–471.e4 (2020). doi: 10.1016/j.molcel.2020.05.032; pmid: 32553192
24. A. Dixit *et al.*, Perturb-Seq: Dissecting Molecular Circuits with Scalable Single-Cell RNA Profiling of Pooled Genetic Screens. *Cell* **167**, 1853–1866.e17 (2016). doi: 10.1016/j.cell.2016.11.038; pmid: 27984732
25. J. M. Replogle *et al.*, Mapping information-rich genotype-phenotype landscapes with genome-scale Perturb-seq. *Cell* **185**, 2559–2575.e28 (2022). doi: 10.1016/j.cell.2022.05.013; pmid: 35688146
26. A. J. Rubin *et al.*, Coupled single-cell CRISPR screening and epigenomic profiling reveals causal gene regulatory networks*Cell* **176**, 361–376.e17 (2019). doi: 10.1016/j.cell.2018.11.022; pmid: 30580963
27. S. E. Pierce, J. M. Granja, W. J. Greenleaf, High-throughput single-cell chromatin accessibility CRISPR screens enable unbiased identification of regulatory networks in cancer. *Nat. Commun.* **12**, 2969 (2021). doi: 10.1038/s41467-021-23213-w; pmid: 34016988
28. O. Ursu *et al.*, Massively parallel phenotyping of coding variants in cancer with Perturb-seq. *Nat. Biotechnol.* **40**, 896–905 (2022). doi: 10.1038/s41587-021-01160-7; pmid: 35058622

Downloaded from https://www.science.org at Broad Institute on April 30, 2026

29. X. Jin *et al.*, In vivo Perturb-Seq reveals neuronal and glial abnormalities associated with autism risk genes. *Science* **370**, eaaz6063 (2020). doi: 10.1126/science.aaz6063; pmid: 33243861
30. C. J. Frangieh *et al.*, Multimodal pooled Perturb-CITE-seq screens in patient models define mechanisms of cancer immune evasion. *Nat. Genet.* **53**, 332–341 (2021). doi: 10.1038/s41588-021-00779-1; pmid: 33649592
31. E. Papalexi *et al.*, Characterizing the molecular regulation of inhibitory immune checkpoints with multimodal single-cell screens. *Nat. Genet.* **53**, 322–331 (2021). doi: 10.1038/s41588-021-00778-2; pmid: 33649593
32. M. Stoeckius *et al.*, Simultaneous epitope and transcriptome measurement in single cells. *Nat. Methods* **14**, 865–868 (2017). doi: 10.1038/nmeth.4380; pmid: 28759029
33. M. P. Gallagher *et al.*, Hierarchy of signaling thresholds downstream of the T cell receptor and the Tec kinase ITK. *Proc. Natl. Acad. Sci. U.S.A.* **118**, e2025825118 (2021). doi: 10.1073/pnas.2025825118; pmid: 34452995
34. J. E. Rood, A. Hupalowska, A. Regev, Toward a foundation model of causal cell and tissue biology with a Perturbation Cell and Tissue Atlas. *Cell* **187**, 4520–4545 (2024). doi: 10.1016/j.cell.2024.07.035; pmid: 39178831
35. M. Zhu, E. Janssen, W. Zhang, Minimal requirement of tyrosine residues of linker for activation of T cells in TCR signaling and thymocyte development. *J. Immunol.* **170**, 325–333 (2003). doi: 10.4049/jimmunol.170.1.325; pmid: 12496416
36. H. Chung *et al.*, Joint single-cell measurements of nuclear proteins and RNA in vivo. *Nat. Methods* **18**, 1204–1212 (2021). doi: 10.1038/s41592-021-01278-1; pmid: 34608310
37. W. Zhang, R. P. Trible, L. E. Samelson, LAT palmitoylation: Its essential role in membrane microdomain targeting and tyrosine phosphorylation during T cell activation. *Immunity* **9**, 239–246 (1998). doi: 10.1016/S1074-7613(00)80606-8; pmid: 9729044
38. B. Yariv *et al.*, Using evolutionary data to make sense of macromolecules with a "face-lifted" ConSurf. *Protein Sci.* **32**, e4582 (2023). doi: 10.1002/pro.4582; pmid: 36718848
39. A. Patil *et al.*, A disordered region controls cBAF activity via condensation and partner recruitment. *Cell* **186**, 4936–4955.e26 (2023). doi: 10.1016/j.cell.2023.08.032; pmid: 37788668
40. H. Lyons *et al.*, Functional partitioning of transcriptional regulators by patterned charge blocks. *Cell* **186**, 327–345.e28 (2023). doi: 10.1016/j.cell.2022.12.013; pmid: 36603581
41. T. Zarin, C. N. Tsai, A. N. Nguyen Ba, A. M. Moses, Selection maintains signaling function of a highly diverged intrinsically disordered region. *Proc. Natl. Acad. Sci. U.S.A.* **114**, E1450–E1459 (2017). doi: 10.1073/pnas.1614787114; pmid: 28167781
42. L. Y. Beh, L. J. Colwell, N. J. Francis, A core subunit of Polycomb repressive complex 1 is broadly conserved in function but not primary sequence. *Proc. Natl. Acad. Sci. U.S.A.* **109**, E1063–E1071 (2012). doi: 10.1073/pnas.1118678109; pmid: 22517748
43. A. S. Holehouse, R. K. Das, J. N. Ahad, M. O. G. Richardson, R. V. Pappu, CIDER: Resources to Analyze Sequence-Ensemble Relationships of Intrinsically Disordered Proteins. *Biophys. J.* **112**, 16–21 (2017). doi: 10.1016/j.bpj.2016.11.3200; pmid: 28076807
44. X. Su *et al.*, Phase separation of signaling molecules promotes T cell receptor signal transduction. *Science* **352**, 595–599 (2016). doi: 10.1126/science.aad9964; pmid: 27056844
45. M. Marasco, T. Carlomagno, Specificity and regulation of phosphotyrosine signaling through SH2 domains. *J. Struct. Biol. X* **4**, 100026 (2020). doi: 10.1016/j.yjsbx.2020.100026; pmid: 32647828
46. M. M. Arbulo-Echevarria *et al.*, A stretch of negatively charged amino acids of linker for activation of T-cell adaptor has a dual role in T-cell antigen receptor intracellular signaling. *Front. Immunol.* **9**, 115 (2018). doi: 10.3389/fimmu.2018.00115; pmid: 29456532
47. S. Müller-Späth *et al.*, From the Cover: Charge interactions can dominate the dimensions of intrinsically disordered proteins. *Proc. Natl. Acad. Sci. U.S.A.* **107**, 14609–14614 (2010). doi: 10.1073/pnas.1001743107; pmid: 20639465
48. E. T. Usher, M. J. Fossat, A. S. Holehouse, Phosphorylation of disordered proteins tunes local and global intramolecular interactions. *Biophys. J.* **123**, 4082–4096 (2024). doi: 10.1016/j.bpj.2024.10.021; pmid: 39539017
49. M. J. Landrum *et al.*, ClinVar: Improving access to variant interpretations and supporting evidence. *Nucleic Acids Res.* **46**, D1062–D1067 (2018). doi: 10.1093/nar/gkx1153; pmid: 29165669
50. C. Kopanos *et al.*, VarSome: The human genomic variant search engine. *Bioinformatics* **35**, 1978–1980 (2019). doi: 10.1093/bioinformatics/bty897; pmid: 30376034
51. K. J. Karczewski *et al.*, The mutational constraint spectrum quantified from variation in 141,456 humans. *Nature* **581**, 434–443 (2020). doi: 10.1038/s41586-020-2308-7; pmid: 32461654
52. P. Angel, K. Hattori, T. Smeal, M. Karin, The jun proto-oncogene is positively autoregulated by its product, Jun/AP-1. *Cell* **55**, 875–885 (1988). doi: 10.1016/0092-8674(88)90143-2; pmid: 3142689
53. M. J. Wither *et al.*, Antigen perception in T cells by long-term Erk and NFAT signaling dynamics. *Proc. Natl. Acad. Sci. U.S.A.* **120**, e2308366120 (2023). doi: 10.1073/pnas.2308366120; pmid: 38113261
54. P. F. Robbins *et al.*, Tumor regression in patients with metastatic synovial cell sarcoma and melanoma using genetically engineered lymphocytes reactive with NY-ESO-1. *J. Clin. Oncol.* **29**, 917–924 (2011). doi: 10.1200/JCO.2010.32.2537; pmid: 21282551
55. G. Li *et al.*, T cell antigen discovery via trogocytosis. *Nat. Methods* **16**, 183–190 (2019). doi: 10.1038/s41592-018-0305-7; pmid: 30700903
56. P. Nicolas *et al.*, Systems-level conservation of the proximal TCR signaling network of mice and humans. *J. Exp. Med.* **219**, e20211295 (2022). doi: 10.1084/jem.20211295; pmid: 35061003
57. R. Evans, M. O'Neill, A. Pritzel, N. Antropova, A. Senior, T. Green, A. Žídek, R. Bates, S. Blackwell, J. Yim, O. Ronneberger, S. Bodenstein, M. Zielinski, A. Bridgland, A. Potapenko, A. Cowie, K. Tunyasuvunakool, R. Jain, E. Clancy, P. Kohli, J. Jumper, D. Hassabis, Protein complex prediction with AlphaFold-Multimer. bioRxiv 2021.10.04.463034 [Preprint] (2022); doi: 10.1101/2021.10.04.463034
58. S. Cho *et al.*, Structural basis for differential recognition of tyrosine-phosphorylated sites in the linker for activation of T cells (LAT) by the adaptor Gads. *EMBO J.* **23**, 1441–1451 (2004). doi: 10.1038/sj.emboj.7600168; pmid: 15029250
59. H. W. H. G. Kessels, A. C. Ward, T. N. M. Schumacher, Specificity and affinity motifs for Grb2 SH2-ligand interactions. *Proc. Natl. Acad. Sci. U.S.A.* **99**, 8524–8529 (2002). doi: 10.1073/pnas.142224499; pmid: 12084912
60. L. Zeng, I. Palaia, A. Šarić, X. Su, PLCγ1 promotes phase separation of T cell signaling components. *J. Cell Biol.* **220**, e202009154 (2021). doi: 10.1083/jcb.202009154; pmid: 33929486
61. D. B. McAffee *et al.*, Discrete LAT condensates encode antigen information from single pMHC:TCR binding events. *Nat. Commun.* **13**, 1–18 (2022). doi: 10.1083/jcb.202009154; pmid: 36460640
62. R. L. Kortum *et al.*, The ability of Sos1 to oligomerize the adaptor protein LAT is separable from its guanine nucleotide exchange activity in vivo. *Sci. Signal.* **6**, ra99 (2013). doi: 10.1126/scisignal.2004494; pmid: 24222714
63. L. B. Case, X. Zhang, J. A. Ditlev, M. K. Rosen, Stoichiometry controls activity of phase-separated clusters of actin signaling proteins. *Science* **363**, 1093–1097 (2019). doi: 10.1126/science.aau6313; pmid: 30846599
64. W. Y. C. Huang *et al.*, A molecular assembly phase transition and kinetic proofreading modulate Ras activation by SOS. *Science* **363**, 1098–1103 (2019). doi: 10.1126/science.aau5721; pmid: 30846600
65. D. Fisch *et al.*, Molecular definition of the endogenous Toll-like receptor signalling pathways. *Nature* **631**, 635–644 (2024). doi: 10.1038/s41586-024-07614-7; pmid: 38961291
66. S. Saitoh *et al.*, The four distal tyrosines are required for LAT-dependent signaling in FcepsilonRI-mediated mast cell activation. *J. Exp. Med.* **198**, 831–843 (2003). doi: 10.1084/jem.20030574; pmid: 12953098
67. F. Facchetti *et al.*, Linker for activation of T cells (LAT), a novel immunohistochemical marker for T cells, NK cells, mast cells, and megakaryocytes: Evaluation in normal and pathological conditions. *Am. J. Pathol.* **154**, 1037–1046 (1999). doi: 10.1016/S0002-9440(10)65356-4; pmid: 10233842
68. J. D. Blair, A. Hartman, F. Zenk, C. Dalgarno, B. Treutlein, R. Satija, Integrated, multi-modal profiling of intracellular protein dynamics in single cells. bioRxiv 2023.03.27.534442 [Preprint] (2023); doi: 10.1101/2023.03.27.534442
69. L. Vistain *et al.*, Quantification of extracellular proteins, protein complexes and mRNAs in single cells by proximity sequencing. *Nat. Methods* **19**, 1578–1589 (2022). doi: 10.1038/s41592-022-01684-z; pmid: 36456784
70. D. Feldman *et al.*, Optical Pooled Screens in Human Cells. *Cell* **179**, 787–799.e17 (2019). doi: 10.1016/j.cell.2019.09.016; pmid: 31626775
71. K. Kappel *et al.*, Characterizing protein sequence determinants of nuclear condensates by high-throughput pooled imaging with CondenSeq. *Nat. Methods* **22**, 1464–1475 (2025). doi: 10.1038/s41592-025-02726-y; pmid: 40524024
72. Z. Zhang *et al.*, A panoramic view of cell population dynamics in mammalian aging. *Science* **387**, eadn3949 (2025). doi: 10.1126/science.adn3949; pmid: 39607904
73. J. Ferreira da Silva *et al.*, Prime editing efficiency and fidelity are enhanced in the absence of mismatch repair. *Nat. Commun.* **13**, 760 (2022). doi: 10.1038/s41467-022-28442-1; pmid: 35140211
74. N. Kim *et al.*, Deep learning models to predict the editing efficiencies and outcomes of diverse base editors. *Nat. Biotechnol.* **42**, 484–497 (2024). doi: 10.1038/s41587-023-01792-x; pmid: 37188916
75. A. J. Hill *et al.*, On the design of CRISPR-based single-cell molecular screens. *Nat. Methods* **15**, 271–274 (2018). doi: 10.1038/nmeth.4604; pmid: 29457792
76. S. F. Banani, H. O. Lee, A. A. Hyman, M. K. Rosen, Biomolecular condensates: Organizers of cellular biochemistry. *Nat. Rev. Mol. Cell Biol.* **18**, 285–298 (2017). doi: 10.1038/nrm.2017.7; pmid: 28225081
77. M. R. Corces *et al.*, An improved ATAC-seq protocol reduces background and enables interrogation of frozen tissues. *Nat. Methods* **14**, 959–962 (2017). doi: 10.1038/nmeth.4396; pmid: 28846090
78. S. Picelli *et al.*, Full-length RNA-seq from single cells using Smart-seq2. *Nat. Protoc.* **9**, 171–181 (2014). doi: 10.1038/nprot.2014.006; pmid: 24385147
79. B. Li *et al.*, Cumulus provides cloud-based data analysis for large-scale single-cell and single-nucleus RNA-seq. *Nat. Methods* **17**, 793–798 (2020). doi: 10.1038/s41592-020-0905-x; pmid: 32719530

Downloaded from https://www.science.org at Broad Institute on April 30, 2026

80. E. K. Brinkman, T. Chen, M. Amendola, B. van Steensel, Easy quantitative assessment of genome editing by sequence trace decomposition. *Nucleic Acids Res.* **42**, e168–e168 (2014). doi: 10.1093/nar/gku936; pmid: 25300484
81. K. F. Cho *et al.*, Proximity labeling in mammalian cells with TurboID and split-TurboID. *Nat. Protoc.* **15**, 3971–3999 (2020). doi: 10.1038/s41596-020-0399-0; pmid: 33139955
82. J. K. Jackman *et al.*, Molecular cloning of SLP-76, a 76-kDa tyrosine phosphoprotein associated with Grb2 in T cells. *J. Biol. Chem.* **270**, 7029–7032 (1995). doi: 10.1074/jbc.270.13.7029; pmid: 7706237
83. J. J. O'Shea, D. W. McVicar, T. L. Bailey, C. Burns, M. J. Smyth, Activation of human peripheral blood T lymphocytes by pharmacological induction of protein-tyrosine phosphorylation. *Proc. Natl. Acad. Sci. U.S.A.* **89**, 10306–10310 (1992). doi: 10.1073/pnas.89.21.10306; pmid: 1279675
84. J. P. Secrist, L. A. Burns, L. Karnitz, G. A. Koretzky, R. T. Abraham, Stimulatory effects of the protein tyrosine phosphatase inhibitor, pervanadate, on T-cell activation events. *J. Biol. Chem.* **268**, 5886–5893 (1993). doi: 10.1016/S0021-9258(18)53403-7; pmid: 8383678
85. C. S. Dobson *et al.*, Antigen identification and high-throughput interaction mapping by reprogramming viral entry. *Nat. Methods* **19**, 449–460 (2022). doi: 10.1038/s41592-022-01436-z; pmid: 35396484
86. J. Pettmann *et al.*, The discriminatory power of the T cell receptor. *eLife* **10**, e67092 (2021). doi: 10.7554/eLife.67092; pmid: 34030769
87. S. Morita, M. K. O'Dair, J. T. Groves, Discrete protein condensation events govern calcium signal dynamics in T cells. bioRxiv 2024.07.31.606035 [Preprint] (2024); .doi: 10.1101/2024.07.31.606035
88. K. B. Wilhelm, A. Vissa, J. T. Groves, Differential roles of kinetic on- and off-rates in T-cell receptor signal integration revealed with a modified Fab'-DNA ligand. *Proc. Natl. Acad. Sci. U.S.A.* **121**, e2406680121 (2024). doi: 10.1073/pnas.2406680121; pmid: 39298491
89. J. J. Y. Lin *et al.*, Mapping the stochastic sequence of individual ligand-receptor binding events to cellular activation: T cells act on the rare events. *Sci. Signal.* **12**, eaat8715 (2019). doi: 10.1126/scisignal.aat8715; pmid: 30647147
90. W. L. Lo *et al.*, Slow phosphorylation of a tyrosine residue in LAT optimizes T cell ligand discrimination. *Nat. Immunol.* **20**, 1481–1493 (2019). doi: 10.1038/s41590-019-0502-2; pmid: 31611699
91. J. Y. Tinevez *et al.*, TrackMate: An open and extensible platform for single-particle tracking. *Methods* **115**, 80–90 (2017). doi: 10.1016/j.ymeth.2016.09.016; pmid: 27713081
92. Y. Hao *et al.*, Integrated analysis of multimodal single-cell data. *Cell* **184**, 3573–3587.e29 (2021). doi: 10.1016/j.cell.2021.04.048; pmid: 34062119
93. T. Stuart, A. Srivastava, S. Madad, C. A. Lareau, R. Satija, Single-cell chromatin state analysis with Signac. *Nat. Methods* **18**, 1333–1341 (2021). doi: 10.1038/s41592-021-01282-5; pmid: 34725479
94. A. Rubin, ShalekLab/Perturb-LAT: v1, Zenodo (2024); doi: 10.5281/zenodo.17428183
95. M. Mirdita *et al.*, ColabFold: Making protein folding accessible to all. *Nat. Methods* **19**, 679–682 (2022). doi: 10.1038/s41592-022-01488-1; pmid: 35637307
96. Y. Lim *et al.*, In silico protein interaction screening uncovers DONSON's role in replication initiation. *Science* **381**, eadi3448 (2023). doi: 10.1126/science.adi3448; pmid: 37590370
97. E. Schmid, Colabfold Batch AlphaFold-2-multimer structure analysis pipeline, Version 1, Zenodo (2023); https://zenodo.org/records/8223143.

ACKNOWLEDGMENTS

We thank members of the Shalek and Regev labs for helpful discussions. We thank J. T. Neal, Bingxu Liu, Matteo Gentili, Rumya Raghavan, Nir Hacohen, Stephanie Gaglione, Michael Birnbaum, and Leslie Berg for sharing experimental resources and guidance. [Figures created using Adobe Illustrator and BioRender.com] **Funding:** Helen Hay Whitney Foundation Research Fellowship (to A.J.R.); United States Department of Agriculture Agricultural Research Service Graduate Student Fellowship (to T.T.D.); NIH NIDA DP1 Avant-Garde Pioneer Award 1DP1DA053731 (to A.K.S.); NIH NIAID 1R01AI149670 (to A.K.S.); Gates Foundation (to A.K.S.); Ragon Institute of MGH, MIT, and Harvard (to A.K.S.); MIT-IBM Watson AI Lab (to A.K.S.); Klarman Cell Observatory at the Broad Institute of MIT and Harvard (to A.R.); NIH NIAID P01 AI091580 (to J.T.G.); Novo Nordisk Foundation Challenge Programme as part of the Center for Geometrically Engineered Cellular Systems NNF17OC0028176 (to J.T.G.); Author contributions: Conceptualization: A.J.R., A.R., and A.K.S. Investigation: A.J.R., T.T.D., A.V.S., and S.C. Funding acquisition: A.K.S., A.R., and J.T.G. Writing: A.J.R., A.R., and A.K.S. Supervision: A.J.R., J.T.G., A.R., and A.K.S. **Competing interests:** A.K.S. reports compensation for consulting and/or SAB membership from Honeycomb Biotechnologies, Cellarity, Parabilis Medicines, Passkey Therapeutics, Ochre Bio, Danaher, Janssen, Relation Therapeutics, IntrECate biotherapeutics, Conquest Technologies, and Dahlia Biosciences unrelated to this work. A.R. is employed by Genentech, Inc., South San Francisco, CA, USA, and has equity in Roche, and is a cofounder and equity holder of Celsius Therapeutics, an equity holder in Immunitas and, until 31 July 2020, was a scientific advisory board member of Thermo Fisher Scientific, Syros Pharmaceuticals, Neogene Therapeutics, and Asimov. **Data, code, and materials availability:** All data needed to evaluate the conclusions in the paper are present in the paper or the Supplementary Materials. Source data for figures is included in data S6. Single-cell ATAC-seq and CITE-seq data are available through the Broad Institute Single Cell Portal via the following accessions: SCP3366, SCP3367, SCP3368, SCP3370, SCP3371, SCP3372. Sequencing reads and processed data are available through the Gene Expression Omnibus (GEO) accession GSE311573. Custom scripts described in the methods are available through Zenodo accession 17428184 (94). Details for the synthesis of materials generated in this study are in the methods section. **License information:** Copyright © 2026 the authors, some rights reserved; exclusive licensee American Association for the Advancement of Science. No claim to original US government works. https://www.science.org/content/page/science-licenses-journal-article-reuse

SUPPLEMENTARY MATERIALS

science.org/doi/10.1126/science.ads6847
Figures S1 to S15; MDAR Reproducibility Checklist; Data S1 to S6

Submitted 23 August 2024; resubmitted 7 July 2025; accepted 27 January 2026

10.1126/science.ads6847

Downloaded from https://www.science.org at Broad Institute on April 30, 2026

Science
AAAS

Disordered protein LAT encodes relative levels of signaling pathways in T cell activation

Adam J. Rubin, Tyler T. Dao, Amelia V. Schueppert, Saehyun Choi, Jay T. Groves, Aviv Regev, and Alex K. Shalek

Science **392** (6797), eads6847. DOI: 10.1126/science.ads6847

Editor's summary

Modular proteins provide a foundation for cellular signaling pathways, allowing integration and specific activation of signaling transduction. However, some scaffold proteins, such as linker for activation of T cells (LAT), have a disordered structure, and how they coordinate the activation of multiple distinct signaling pathways is not well understood. Rubin *et al*. used a systematic approach to define regions of LAT important for specific protein-protein interactions. Sequence element mutations that blocked interaction with one partner protein also disrupted the binding and downstream signaling of others. This finding suggested that, rather than organizing discrete modules, LAT assembled a signalosome in which its interaction partners helped hold the complex together, allowing the coordinated activation of multiple signal transduction pathways. —Sarah H. Ross

View the article online

https://www.science.org/doi/10.1126/science.ads6847

Permissions

https://www.science.org/help/reprints-and-permissions

Downloaded from https://www.science.org at Broad Institute on April 30, 2026

Use of this article is subject to the Terms of service

Science (ISSN 1095-9203) is published by the American Association for the Advancement of Science. 1200 New York Avenue NW, Washington, DC 20005. The title *Science* is a registered trademark of AAAS.

Copyright © 2026 The Authors, some rights reserved; exclusive licensee American Association for the Advancement of Science. No claim to original U.S. Government Works